Update on The Science and Technology of Diesel Particulate Filters †

Athanasios G. Konstandopoulos[1,2]* and Eleni Papaioannou[1]
Aerosol & Particle Technology Laboratory[1]
Department of Chemical Engineering, Aristotle University of Thessaloniki[2]

Abstract

As diesel emission regulations become more stringent, diesel particulate filters (DPFs) have become possibly the most important and complex diesel emission control device. This paper provides an update on the science and technology of diesel particulate emission control, drawing from the results of many research projects carried out by the authors in collaboration with the automotive industry and its suppliers. Both fundamental as well as application-oriented approaches are presented to study the physicochemical characteristics of diesel soot particles and soot deposits formed in DPFs, which are viewed as multifunctional separators/reactors. Theroretical and experimental aspects of filtration efficiency, pressure drop, ash accumulation and soot reactivity (with emphasis on catalyst-assisted soot oxidation) are addressed, employing systems ranging from small-scale filter samples to full-scale devices installed in the exhaust system of diesel engines. Properly combined, the current state of knowledge, experimental methods and simulation approaches all provide a rational and systematic route for enhancing the design and reliability of future diesel particulate emission control systems.

Keywords: diesel particulate filter, emission control, filtration, soot, catalytic oxidation, simulation

1. Introduction

Advanced fuel injection technology in conjunction with an inherent high thermal efficiency have led to an increased market share of diesel-powered vehicles especially in Europe, and the trend is expected to continue assuming the diesel engine is able to meet ever more stringent emission limits in the future. This is dependent on the employment of cost-efficient, advanced emission control systems for particulate and NO_x emissions. However, the adverse health effects of combustion-generated nanoparticles such as diesel soot generate a highly visible public debate where the role of aerosol scientists and technologists becomes very important both in terms of measurement and assessment technologies as well as technological solution developers/providers.

† Accepted: August 23, 2008
1 CERTH/CPERI, PO Box 361, Thermi, 57001 Thessaloniki, Greece.
2 Thessaloniki, Greece
* Corresponding author
E-mail: agk@cperi.certh.gr

Particulate emission control entails measures to reduce both the solid (soot) particle emissions and the liquid particle (droplet) emissions formed due to condensation of the exhaust as it cools down. The latter can be easily reduced by regulating their precursors (reducing the fuel sulfur level and installing advanced diesel oxidation catalysts to oxidize the complete spectrum of hydrocarbon (HC) emissions). The solid soot emissions, however, remain intimately connected with the nature of the diesel combustion process, and their reduction can be achieved either by in-cylinder measures improving the combustion process itself, or by employing aftertreatment systems such as diesel particulate filters (DPFs). As diesel emission regulations become more stringent, the use of DPFs increases progressively in both light-duty/passenger car and heavy-duty/commercial vehicle applications. DPFs represent an important and highly complex type of multifunctional chemical reactor combining multiphase, separation, chemical reactions and material transformations over many disparate temporal and spatial scales (**Fig. 1**).

Modern DPFs exhibit very high filtration efficien-

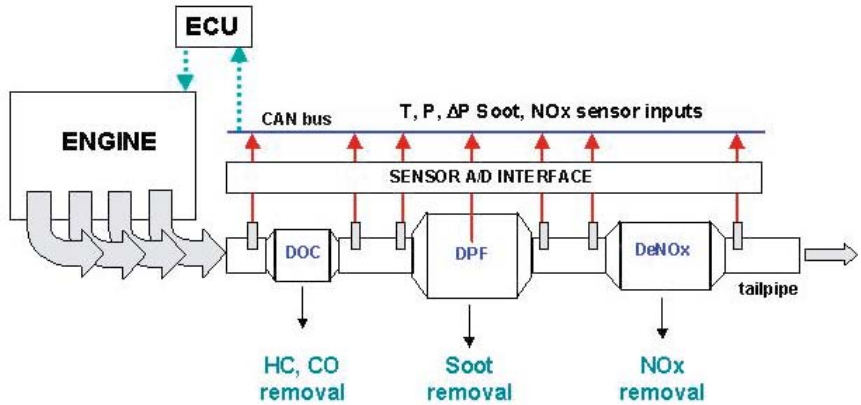

Fig. 1 Example of integrated soot-NO_x emission control system. DPF stands for diesel particulate filter. Sensory inputs of temperature (T), pressure (P), pressure drop (ΔP), soot and NO_x concentration will be required along the exhaust pipe.

cies, however, they need to be periodically cleaned (regenerated) in order to achieve efficient and safe operation of the vehicle. As typical diesel exhaust conditions are not hot enough to initiate and maintain particulate (soot) oxidation, active (engine) means are employed to raise the exhaust gas temperature up to the point that particulate oxidation can be self-sustained in the filter at fast enough rates (>650 C). To achieve the oxidation of soot particles at lower temperatures (250 – 550 C), a number of direct and indirect catalytic measures can be employed ranging from fuel additives, generation of reactive species, catalytic combustion of post-injected fuel and filter coatings promoting soot oxidation.

Modern trends[1, 2, 3, 4] in passenger car emission control systems are now focusing on so-called "fit-for-life" solutions, thus overcoming the need for servicing (ash removal) of the DPF during the vehicle lifetime. Robustness and durability of the engine and emission control system is also clearly a first priority in heavy-duty surface transportation. These trends pose specific challenges and create new opportunities in the area of diesel emission control technology.

State-of-the-art diesel emission control systems are complex assemblies of chemical reactors and separators, sometimes integrating different functionalities on the same monolithic support to achieve demanding requirements in space and cost, especially in passenger cars[5, 6, 7] . Such complex emission control systems require advanced simulation tools for their cost-effective design, development, system-level integration and optimization. In addition, requirements for robust on-board monitoring and control generate the need for efficient algorithms which are implementable in computationally limited engine control units (ECUs) and which will provide accurate knowledge of the state of the emission control system during vehicle operation, and which can be used in control loops for management of the integrated powertrain-emission control system.

In the present paper, we provide an overview of our work in the area of diesel particulate emission control technologies, drawing from an over ten-year participation in several research projects in collaboration with the automotive industry and its suppliers.

The structure of the paper is as follows: Initially, we discuss the physicochemical characteristics of diesel soot and then descibe the operation of a DPF as a separator, addressing its filtration efficiency and pressure drop behavior. We then discuss the operation of the DPF as a reactor and address the regeneration process (the oxidation of accumulated soot by various techniques, with emphasis on catalyst-assisted soot oxidation). Subsequently, we discuss the application of advanced simulation methods to DPF systems and provide the conclusions of this study.

2. Diesel Soot

The characterization of soot particles emitted from modern diesel engines is a prerequisite for any particulate emission control approach, and has attracted enormous interest in the literature, with some representative recent studies being those in reference[8, 9].

From a control technology point of view, we are interested in the state of the soot particles in the raw exhaust upstream of the DPF. Depending on the exhaust temperature, organic components from the lubrication oil and/or the fuel could condense on the soot particles and form the so-called soluble organic fraction (SOF) of diesel particulate. However, this is typically a phenomenon occurring upon dilution of

the exhaust, sometimes leading to the formation of additional particles, the so-called nucleation mode [9]. A high-SOF-content soot is sometimes referred to as "wet soot", and a low-SOF-content soot as "dry soot". It should be noted though, that reference to the SOF content of diesel particulate matter almost always implies particulate matter sampled on a Teflon–coated filter after a relatively long residence time and a dilution process in a dilution tunnel at a temperature of 52℃, just as the legislated sampling protocols stipulate.

It must be borne in mind that sampling lines and flame ionization analyzers for hydrocarbon emissions measurements from the exhaust typically operate at 190℃ to avoid condensation-induced sampling artifacts. In studies of diesel particulates under raw exhaust conditions using gravimetric raw exhaust sampling techniques[10], it was observed that at an exhaust temperature of 350℃ no particle-bound SOF was present.

Most modern DPF systems are preceded by a diesel oxidation catalyst (DOC), which is employed to oxidize exhaust hydrocarbons (injected in the engine cylinder or in the exhaust) and thus raise the exhaust temperature to the levels needed for DPF regeneration. The DOC almost eliminates any SOF that might be present on the soot particles, hence for the remainder of this paper, the term soot particle will imply the *predominantly solid aggregates* that exist in diesel exhaust (also known as the accumulation mode particles[9].

The available measurements indicate that the majority of emitted solid diesel aggregate particles have electrical mobility and aerodynamic diameters in the range of 10-300 nm. Primary particle diameters are found to lie in the range of 8 to 40 nm[8, 9, 11].

The composition and morphology of diesel soot particles in the raw exhaust is very important, as this is the aerosol that challenges the DPF. The morphology of the soot particles affects the structure of deposits[12] that are formed in the DPF (hence the engine backpressure), while their composition (which is predominantly carbonaceous) affects their oxidation potential and hence the ease of DPF regeneration[13, 14, 15, 16, 17]. The substructure of soot primary particles obtained by different combustion sources and fuels has been studied by high-resolution transmission electron microscopy (TEM)[13, 14, 15, 18, 19], and it is connected to the soot reactivity.

Harris and Maricq[20] have shown that soot particle size distributions from various types of diesel engines (model years from 1995-1998), running on different fuels under a wide range of operating conditions, can be approximated by a "signature distribution" when the number-based particle size distribution (PSD) is normalized with respect to the total particle number concentration and the particle size is scaled with respect to the mean particle size. We refer to this way of presentation as Harris-Maricq (HM) coordinates. More recently[21, 22], we have measured soot size distributions from the exhaust of 5 turbo-charged, direct-injection diesel engines (model years 1997-2003) with displacements in the 1.9-2.4L range and advanced fuel-injection systems (3 common-rail, one pump unit injector, and one rotary-pump-based fuel-injection system). Particles were measured employing a Scanning Mobility Particle Sizer (SMPS) and a Long Path Multi-wavelength Extinction (LPME) analyser as described in[11], and the obtained size distributions are plotted in **Fig. 2**, in HM coordinates. The average value of σ_g for each engine (operating at several steady state points) is also given in **Fig. 2**. A remarkable constancy of σ_g is observed, $\sigma_g = 1.89 \pm 0.08$. When the Harris and Maricq[20] data are included, all data are consistent to within 4% with a constant shape for the particle size distribution with an average $\sigma_g = 1.84$. The constant shape for the size distribution arises as the steady state solution of the soot aggregate population balance that accounts for coagulation and oxidative fragmentation processes [21].

The oxidative fragmentation of soot particles has been observed in flame studies by[23] and limits further aggregate growth. The resulting soot fragments re-collide with the soot aggregates, leading to the establishment of a steady state at which point coagulation balances fragmentation and therefore the emergence of a size distribution with a "constant shape". Naturally the simultaneous occurrence of these two processes will lead to a distribution of soot aggregate morphologies. It is well known that diffusion limited cluster-cluster aggregation, (DLCCA), a much-studied growth mechanism[24, 25, 26], leads to aggregate structures with a $D_f = 1.8$, while diffusion limited aggregation (DLA) (a growth mechanism where monomers collide with clusters) leads to aggregate structures with a $D_f = 2.5$. Employing a simultaneous measurement of electrical-mobility-based and aerodynamic-diameter-based distributions, we plot in **Fig. 3** how the fractal dimension of diesel soot aggregates is distributed according to their electrical mobility diameter, as presented in[27].

We observe a very robust pattern over the different engines and operation conditions tested, namely that small soot particles have a nearly spherical/

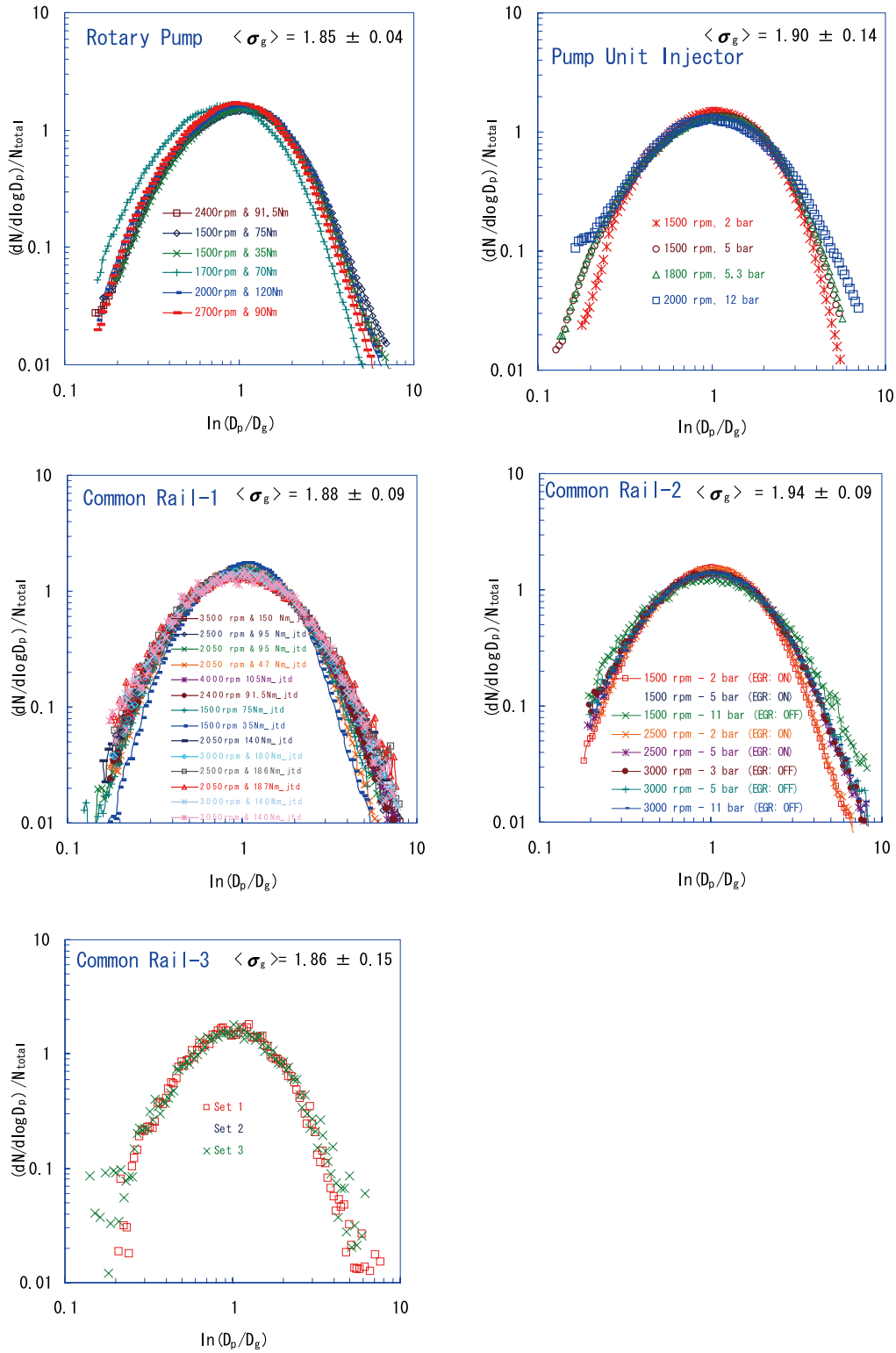

Fig. 2 Measured soot PSDs for five different engines at several operation points. N is the particle number concentration, D_p the particle diameter, D_g the geometric mean particle diameter and σ_g the geometric standard deviation of the PSD.

compact morphology (D_f = 3) which rapidly evolves toward the value D_f= 1.8 (the DLCCA limit) as the soot aggregate size increases up to about 100 nm. Then further increase of the aggregate size leads

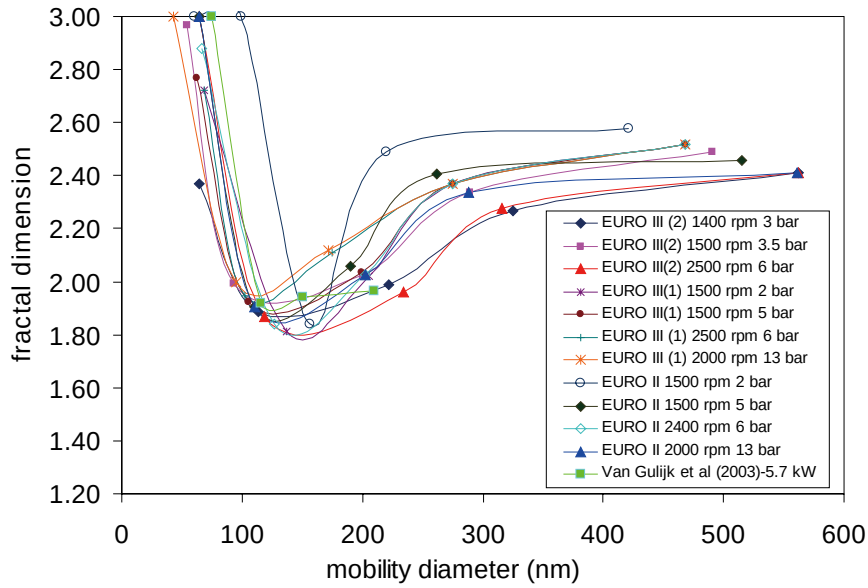

Fig. 3 Fractal dimension of soot aggregates with different mobility diameters obtained with different engines and operating conditions. Measurements from one Euro II and two Euro III diesel engines and a diesel generator [29] as presented in [27].

to an increase of D_f to a range of around 2.4-2.5. As mentioned above, such a fractal dimension is consistent with a mechanism of addition of monomers to a cluster, and we rationalize it by considering the removal by oxidative fragmentation of smaller units from a large soot aggregate and their subsequent recollision with the same or other aggregates, through a type of DLA process. The data are consistent with an overall average $D_f = 2.4$, and a similar average D_f has been obtained by[28], among others.

In[21] it is shown that in principle, σ_g does not have a universal value but rather depends on the soot aggregate morphology (as described by the soot aggregate fractal dimension, D_f) and the mode of the oxidative fragmentation process (e.g. attrition, random fragmentation, equal size fragmentation, etc). An average fractal dimension $D_f = 2.4$ for the diesel soot aggregates [28] and a physically realistic random fragmentation mode are shown to be consistent in [21] with the experimentally observed values of σ_g. An explicit connection between the combustion process, the aggregate morphology and the easily measured σ_g can therefore be made.

3. The DPF as a Separator: Filtration and Pressure Drop

Filters separate the diesel soot aggregates from the exhaust by means of a variety of transport mechanisms. The main deposition mechanisms are those of Brownian diffusion and direct interception, while thermophoresis can be important in the presence of temperature gradients[30]. Over the last 20 years, many DPF system concepts have appeared which incorporate different filter media and geometric configurations, regeneration technologies and control/monitoring options. The interested reader should consult the literature[31, 32, 33] as well as on-line databases[34].

1) Filter media and configurations

The filter media and geometric configuration is a key element in the DPF system, and the selection process calls for a careful balancing of different criteria including pressure drop performance, particulate collection efficiency, regeneration, durability and cost. Geometric configurations of filters are listed in **Table 1**[35, 36].

The wall-flow monolith honeycomb design originally introduced in 1981[37] still remains the most popular configuration, since it is a very compact arrangement, thus exhibiting a low pressure drop without having to make sacrifices in filtration rate or available space.

Representative material properties are given in[36].

Since the majority of filter configurations use some sort of wall-flow arrangement, we will focus our investigation for the remaining of the paper on the wall-flow geometry and honeycomb structures. It should be noted though that the developments/results can be extended direct to the other geometries[38]. In the following text, we examine the factors that affect the

Table 1 Diesel Particulate Filter Materials and Configurations

Ceramic	
Oxide ceramics	
• Cordierite	• Extruded honeycomb wall-flow monoliths
• Mullite	• Extruded honeycomb wall-flow monoliths
• Aluminum titanate (tialite)	• Foam monolithic blocks and plates
	• Extruded honeycomb wall-flow monoliths
Non-oxide ceramics	
• Recrystallized silicon carbide	• Extruded honeycomb wall-flow monoliths
• Silicon-bonded silicon carbide	• Fibrous felts
• Silicon nitride	• Extruded honeycomb wall-flow monoliths
	• Extruded honeycomb wall-flow monoliths
Metallic	
• Sintered metal powder	• Pleated wall-flow sheets
• Metal fiber	• Fibrous felt elements and cartridges
• Metal foam	• Sheets and cartridges

pressure drop and filtration efficiency of DPFs.

2) Filtration theory

The first applications and validations of filtration theory to diesel particulate filters were made in[39] for fibrous structures and in[30] for wall-flow extruded filters. As flow in porous media represents a challenging area of fluid mechanics, initial approaches[39, 40, 41] have employed so-called unit-cell models where the porous filter wall is approximated as a collection of "cells", each hosting an object of simple geometry (a sphere for granular filters and a cylinder for fibrous filters). In these studies, it was shown that the classic filtration theory employing the concept of the "unit collector" (spheres for extruded filters and cylinders for fibrous and foamy structures) can give a good estimate of the size-specific collection efficiency of "clean" DPFs with respect to solid particles.

Fig. 4 demonstrates that application of the unit-cell filtration theory can successfully describe the emitted size distribution of diesel aggregates at the DPF outlet for widely varying pore sizes of prototype SiC-based extruded wall-flow monoliths with a porosity of 42%.

To account for the effect of particle accumulation on the filtration process, the unit-cell-based filtration theory was extended to include a local recomputation of the evolving unit-cell geometry (**Fig. 5**) caused by deposition of particles[35]. The transient filtration model derived was tested with very good agreement against experimental data with ceramic, metallic and fibrous filters, see for example[42]

3) Flow resistance and pressure drop of filters

Based on the fundamental principles of fluid mechanics and flow through porous media, Konstandopoulos and Johnson[30] published the first analytical solutions for the flow fields and pressure drop of wall-flow monoliths in terms of the filter media microstructure and geometric configuration that were validated experimentally for a particular extruded monolith design. The analytical model (extended for non-Darcian flow effects) was later shown to be in excellent agreement with 3-D computational fluid dynamics (CFD) simulations and was further validated against a larger variety of filter media[42, 43, 44]. The Konstandopoulos and Johnson[30] model has been extensively tested against a variety of filter samples, and it is reported to give excellent *a-priori* predictions of the pressure drop, opening up new development possibilities[41, 45, 46].

The approach was later extended to include the influence of the accumulated soot accounting explicitly for the soot layer microstructure and its dependence on the operating conditions of the DPF[12, 47]. In the present section, we outline the dominant factors that are responsible for the pressure drop of clean and soot-loaded DPFs[48].

3.1 Clean filters

Based on previous work in the area[30, 35, 40, 43, 49, 50], the flow resistance of a clean DPF as expressed by its pressure drop can be very accurately described by totalling the individual pressure drop contributions, shown in **Fig. 6**. Each contribution to the pressure drop requires the specification of one or more parameters, which collectively define the required set of what we term "flow resistance descriptors".

Flow resistance descriptors of DPF walls, experimental protocols for their determination and useful correlations have already been presented in[48]. The thin porous wall contributes a pressure drop that is described by the sum of a Darcy term and a so-called Forchheimer term[30, 35, 40, 47, 49]

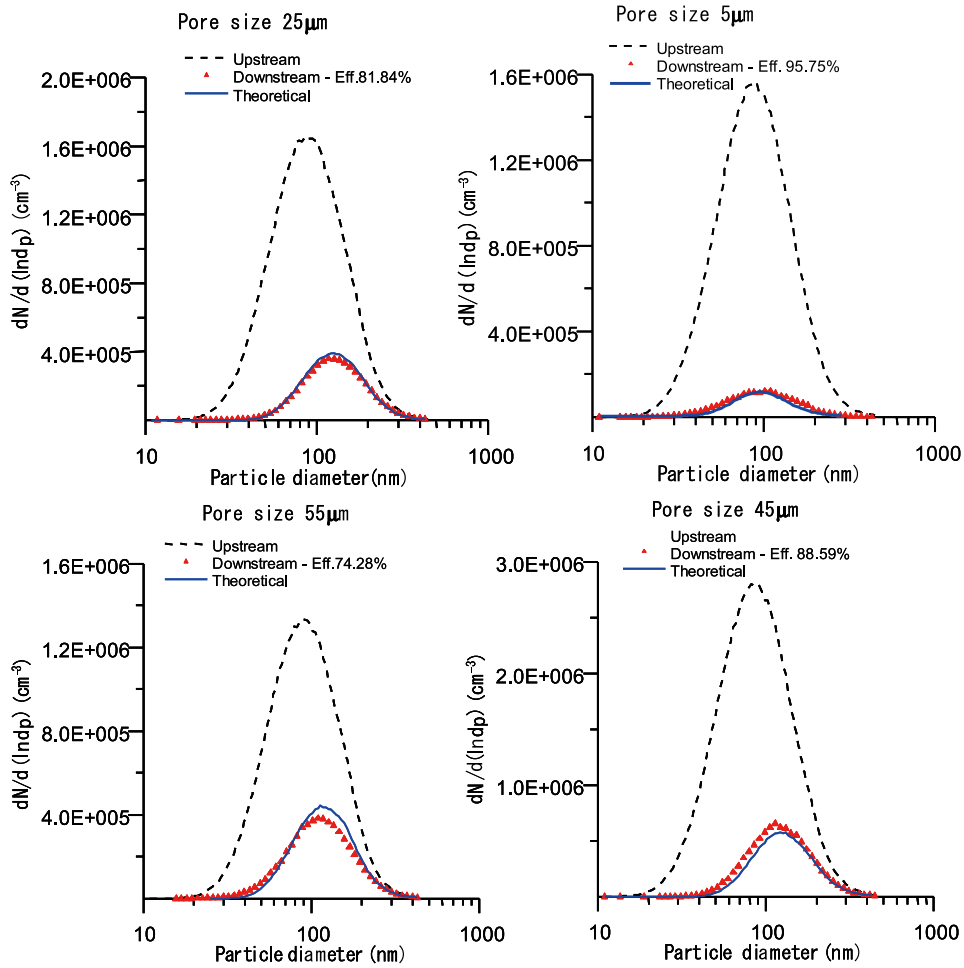

Fig. 4 Effect of pore size on the size distribution of emitted soot aggregates. The DPFs tested are prototype SiC-based extruded wall-flow monoliths with a porosity of 42%. The theoretical lines are the predictions of the unit-cell-based filtration theory [30, 35]

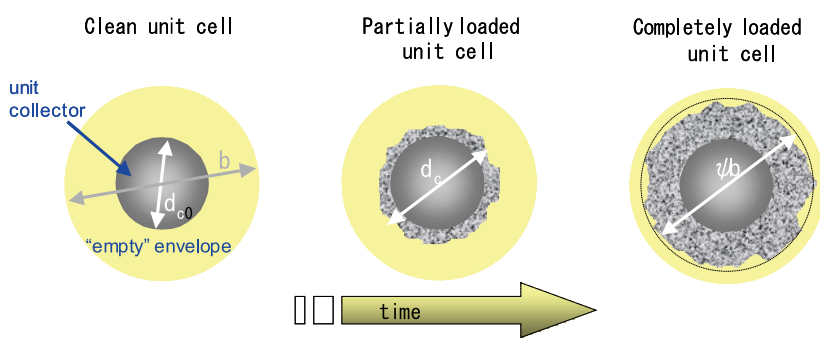

Fig. 5 Unit-cell filtration model. The collector size dc and the empty envelope b are matched to the macroscopic porosity of the filter. The unit-cell blocks when the size of the collector becomes a fraction ψ of b [35, 42]

$$\Delta P_{wall} = \underbrace{\frac{\mu}{k} u_w w_s}_{Darcy} + \underbrace{\beta \rho u_w^2 w_s}_{Forchheimer} \qquad \text{Eq. 1}$$

The parameters appearing in Eq. 1 that need to be specified to permit estimations of the pressure drop are the Darcy permeability k and the Forchheimer coefficient β. The permeability has dimensions of length squared, and $k^{1/2}$ represents a pore level length scale, characteristic of the porous medium. It should be emphasized that the permeability and the

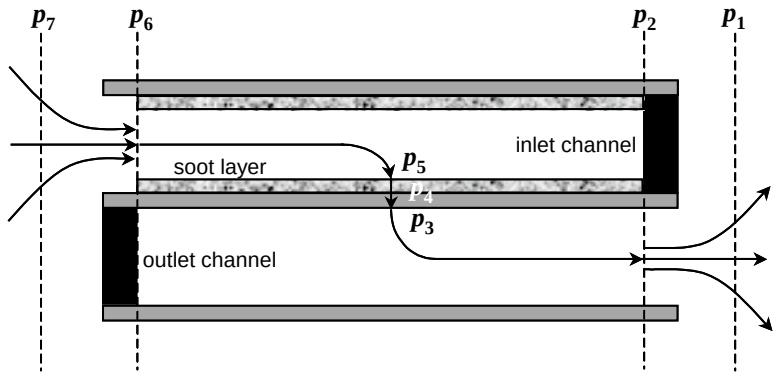

Fig. 6 Schematic of channels adjacent to filter inlet and outlet depicting local pressure values for the derivation of the effects of compressibility on pressure drop.

Forchheimer coefficient are *intensive* properties of the porous medium and for a homogeneous medium, will not depend on the size of the sample measured.

In our past work[30, 35, 47], we have introduced and validated a generalized representation for the permeability of DPFs, which can be stated as:

$$k_{wall} = f_w(\varepsilon) \cdot d_c^2 \cdot SCF(d_c) \qquad \text{Eq. 2}$$

where $SCF = 1 + Kn\left(1.257 + 0.4e^{-1.1/Kn}\right)$ is the Stokes-Cunnigham factor[51] accounting for slip-flow effects that are dependent on the local value of the Knudsen number of the flow through the porous filter wall, $Kn = 2\lambda/d_c$ (based on the prevailing mean free path λ and the typical grain diameter dc of the filter media), and the hydrodynamic interaction function $f_w(\varepsilon)$ for sintered granular media was derived in several interchangeable forms[48].

$$f_w(\varepsilon) = \begin{cases} 0.09 \times f(\varepsilon) = 0.09 \times \frac{2}{9} \cdot \frac{\left[2 - \frac{9}{5} \cdot (1-\varepsilon)^{1/3} - \varepsilon - \frac{1}{5} \cdot (1-\varepsilon)^2\right]}{(1-\varepsilon)} \\ \\ \frac{\varepsilon^3}{585 \times (1-\varepsilon)^2} \\ \\ 0\{.018 \times \varepsilon^{4.34} \end{cases} \qquad \text{Eq. 3}$$

Slip-flow phenomena are not usually observed in bare (uncoated) DPFs since the pore/grain size of these filters is sufficiently greater than the gas mean free path. For some catalyst-coated filters, however, temperature-dependent slip-flow effects may cause the pressure drop to become smaller than that predicted from continuum flow. In this case, and as shown in[35], one can employ a slip-flow-corrected permeability of the coating, $k_{coating}$. that depends on the local value of the Knudsen number of the flow through the coating, $Kn = 2\lambda/d_{grain}$ where d_{grain} is a characteristic length scale of the coating (which usually has a granular character). $k_{coating} = f(\varepsilon) \times d_{grain}^2 \times SCF$

The Forchheimer coefficient has dimensions of inverse length. Both k and β can then be related to a "pore size" (which is operationally defined by the employed measurement technique) and porosity of the porous medium. In[48] it was shown that the Forchheimer coefficient β and the Darcy permeability k were interrelated according to:

$$\beta = \frac{const.}{\varepsilon^{1.5}\sqrt{k}} \qquad \text{Eq. (4)}$$

The value of the constant in Eq. (4) will depend on the actual morphology of the elements making up the porous medium. Based on the known structural properties of commercially available wall-flow DPFs (porosity in the order of 50% and pore size in the 10-30 μm range) and ranges of DPF operating flow rates, it can be assumed that the Forchheimer contribution to the pressure drop will be negligible, unless filters are operated at relatively high filtration velocities. This can occur for some newer filter designs based on sheets of sintered metal, fibrous materials or foam structures. From experiments with granular sintered metal filter media[38] the value of the constant was found to be equal to 0.34, while from experiments with high-porosity fibrous filter media, the constant was evaluated to be 16.6[47].

Additional pressure drop occurs in a wall-flow filter due to frictional losses of the flow along the square channels of the filter. This pressure loss has a linear dependence on channel velocity for laminar flow, in a square channel of inlet opening a and length L, according to:

$$\Delta P_{friction} = \frac{\mu U L}{a^2} 2 c_f \mathrm{Re} \xi \qquad \text{Eq. 5}$$

where c_f Re, for fully developed laminar flow in a

square cross-sectional channel, has a constant value of 14.227, and in our notation we designate:

$$F=2c_f\mathrm{Re} \qquad \text{Eq. 6}$$

The assumption of fully developed laminar flow is usually satisfied in a wall-flow filter since the Re number based on the channel opening is typically less than 1000 for a DPF measuring 5.66 inches $\times$6 inches and with 200 cells/in^2(cpsi). The factor ξ is a correction accounting for the effect of strong suction or injection on c_f Re. For typical wall-flow filter applications, ξ can be taken as equal to 1 since local wall-flow velocities u_w are small enough to keep the wall Re number ($u_w a\,\rho/\mu$) less than 2 [30].

Finally, there are inertial losses due to contraction and expansion of the flow as it enters and leaves the filter channels. This component increases with the axial channel inlet velocity U according to:

$$\Delta P_{contr./expan.} = \zeta\frac{\rho U^2}{2} \qquad \text{Eq. 7}$$

where ζ is the so-called contraction/expansion inertial loss coefficient, which in general depends on the filter fractional open cross sectional flow area and on the Reynolds number[47]. All these contributions are included in the following equation that gives the total pressure drop of a clean wall-flow filter:

$$\Delta P = \frac{\mu Q}{2V_{DPF}}(a+w_s)^2\left[\frac{w_s}{ka}+\frac{8FL^2}{3a^4}\right]+\frac{\rho Q^2(a+w_s)^4}{V_{DPF}^2a^2}\left[\frac{\beta w_s}{4}+2\zeta\left(\frac{L}{a}\right)^2\right] \qquad \text{Eq. 8}$$

Eq. 8 has been shown to be a predictive and validated macroscopic model for the pressure drop of wall-flow filters[30, 35, 40, 43, 49, 50], and requires as input the flow rate Q, the filter geometrical characteristics (V_{DPF}, a, ws. L), the wall permeability k and the filter inertial loss coefficient, ζ. Eq. 8 can then be employed in conjunction with experimental data to determine the relevant flow resistance coefficients k and ζ, provided that all other parameters entered in Eq. 8 are known or can be independently measured.

The estimation of k can also be attempted from the filter microstructure, employing any of a number of idealized geometrical descriptions of the porous medium structure, an approach that was used in the past[48]. In that case, the required input data are the "porosity" and "pore size", parameters that are themselves operationally defined based on the measurement technique. Such estimations, however, based as they are on idealized geometrical representations of the filter microstructure, provide only order-of-magnitude estimates of the wall permeability. True-to-the-geometry representations based on statistical computer reconstruction of the porous filter wall from microscope pictures and subsequent computational analysis of the flow through the wall have been introduced in[47, 48, 52] and provide more accurate estimates.

Experiments for direct measurements of wall permeability can be performed using either filter disks of the same material formulation[35] or pieces from the filter wall, after the orthogonal walls have been removed carefully[53]. Such experiments are quite time-consuming and are not easy to employ for the routine analysis of samples. An easier, non-destructive alternative for determination of the permeability of a wall-flow filter sample is to rely on careful experimental measurements made on complete honeycombs and the application of predictive, continuum-level mathematical models, such as Eq. 8. This is now standard industrial practice[54].

For the determination from first principles of the inertial losses coefficient, ζ, the use of three-dimensional CFD simulation has already proved to be promising[47]. However, the computational effort required for an extensive parametric study of a multi-channel configuration[47] makes experimental testing a more flexible alternative.

3.2 Soot-loaded filters

Depending on their microstructure, filters can exhibit more a so-called deep bed filtration mode or a so-called cake (or surface) filtration mode[55]. With reference to **Fig. 7**, the deep-bed filtration mode occurs initially (i.e. all filter structures will exhibit it) and is characterized by a non-linear increase of the filter pressure drop as a function of the accumulated soot mass in the filter. This is due to the initial deposition of soot particles inside the porous structure of the filter wall, which block the flow paths locally. Depending on the microstructure of the porous filter, even a small amount of deposited soot may have a huge effect on the pressure drop, since it may block a disproportionately large part of the pore structure, hence the non-linear character of the pressure drop evolution. As the porous wall becomes more and more blocked by the deposited soot, there is a smooth transition to the cake filtration mode, where a macroscopic soot layer grows on top of the filter wall, characterized by a linear dependence of the pressure drop on the accumulated particulate mass in the filter.

It is obvious that more porous wall structures will exhibit a more pronounced deep-bed mode of filtration, however, in all filter structures that are currently commercially employed for DPFs, a cake

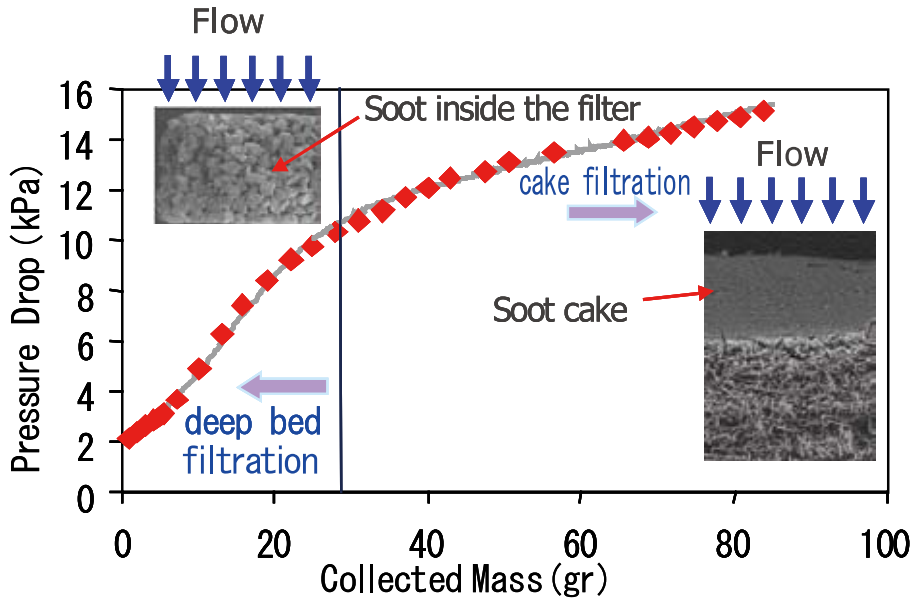

Fig. 7 Filtration modes: from deep-bed to cake (surface) filtration.

mode of filtration eventually sets in, since the amount of soot one might want to be stored in the DPF before its regeneration is initiated is higher by far than the amount that the porous wall can accommodate. Typically, the porous wall will store between 0.5-2 g/m^2 of soot mass per filtration area (depending on the filter structure), while the total amount of soot stored before regeneration is on the order of 10 g/m^2 (depending on the employed DPF material and configuration).

For predominantly cake-mode-type DPFs, a closed-form expression has been derived for the pressure drop as a function of soot loading[35].

The soot-loaded DPF pressure drop is expressed in terms of a uniform, effective soot deposit thickness, w on the filter wall[35], which with reference to **Fig. 8** is computed as follows:

$$w = \frac{\alpha - \sqrt{\alpha^2 - \frac{m_{soot}}{N_{cells} L \rho_{soot}}}}{2} \qquad \text{Eq. 9}$$

$$\Delta P = \frac{\mu Q}{2V_{DPF}}(a+w_s)^2\left[\frac{w_s}{k_o\alpha} + \frac{1}{2k_{soot}}\ln\left(\frac{\alpha}{\alpha-2w}\right) + \frac{4FL^2}{3}\left(\frac{1}{(\alpha-2w)^4} + \frac{1}{\alpha^4}\right)\right] + \frac{\rho Q^2(\alpha+w_s)^4}{V_{DPF}^2\alpha^2}\left[\frac{\beta w_s}{4} + 2\zeta\left(\frac{L}{\alpha}\right)^2\right] \qquad \text{Eq. 10}$$

The analytical expression for the DPF pressure drop has been extensively validated (**Fig. 9**) against 3-D CFD and experimental results [35].

Fig. 10 depicts the experimental transient loading behavior of different DPFs and their simulation using the transient filtration model of Konstandopoulos et al.[35].

Whenever the DPF pressure drop is significant when compared to the atmospheric pressure, compressibility effects need to be taken into account. The DPF pressure drop in the case of compressible flow has been analyzed in[48] as explained in the Appendix.

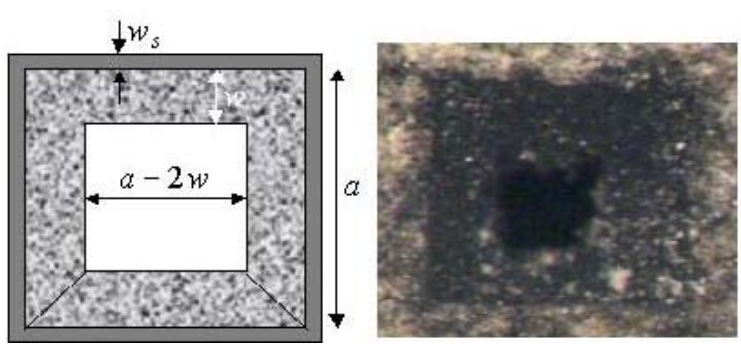

Fig. 8 Schematic and nomenclature of soot cake accumulation inside the cross-section of a channel (left) and image of soot accumulated in a DPF channel (right).

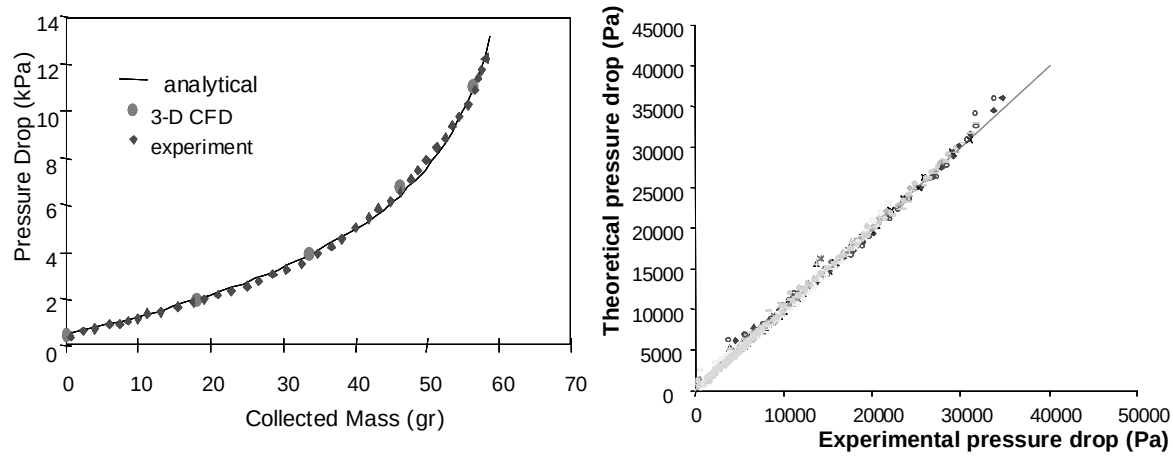

Fig. 9 Validation of an analytical pressure drop model with 3-D CFD (left) from [35], and experiments (right) with 10 filters in 31 experimental runs with light- and heavy-duty diesel engines from [43].

3.3 Soot deposit microstructure

Konstandopoulos et al. [12] demonstrated for the first time that during filter loading, the microstructure of the soot cake is determined by the relative strength of convective vs. diffusive transport of the soot aggregates towards the deposit **Fig. 11**. The soot cake packing density (ρ_{soot}) and permeability (k_{soot}) were therefore shown to be not just "static" intrinsic physical properties of the soot cake, as it was commonly assumed in the literature. They were instead shown to be "dynamic" material properties of the soot porous cake that depend on the deposit growth mechanism and its history, and that they are determined by the prevailing value of the dimensionless mass transfer Peclet number, $Pe = u_w\, d_{pr}/D_p$, where d_{pr} is the primary particle size of the soot aggregates and D_p is the soot aggregate diffusion coefficient.

The soot cake packing density (ρ_{soot}) and permeability (k_{soot}) can be related to the porosity ε and primary particle size (d_{pr}) of the soot aggregates as follows[12]:

$$\rho_{soot} = \tilde{\rho} \cdot (1-\varepsilon) \qquad \text{Eq. 11}$$

$$k_{soot} = f(\varepsilon) \cdot d_{pr}^2 \cdot SCF \qquad \text{Eq. 12}$$

where SCF is the Stokes-Cunningham factor calculated with a Knudsen number (K_n) based on the primary soot particle size (d_{pr}) from:

$$SCF = 1 + Kn \cdot (1.257 + 0.4e^{-1.1/Kn}) \qquad \text{Eq. 13}$$

and $f(\varepsilon)$ is the Kuwabara hydrodynamic function which depends on the porosity ε, through[30, 55]:

$$f(\varepsilon) = \frac{2}{9} \cdot \left[\frac{2 - \frac{9}{5}(1-\varepsilon)^{1/3} - \varepsilon - \frac{1}{5}(1-\varepsilon)^2}{(1-\varepsilon)} \right] \qquad \text{Eq. 14}$$

Further insight into soot cake properties has been obtained by model experiments with soot aggregates generated by a Combustion Aerosol Standard (CAST) burner (Matter Engineering, Switzerland). The CAST is a quenched diffusion flame gas (propane) burner that allows the stable and controlled generation of soot aggregates over a much larger size range than that found in diesel exhaust. **Fig. 12** depicts the hydrodynamic resistance factor $(\rho \times k)_{soot}$ of CAST soot-deposited cakes on flat disk-shaped glass-fiber filters as a function of the Peclet number and aggregate mobility diameter d_{ag}.

The values of the aggregate mobility diameters shown in **Fig. 12** are values measured by the Scanning Mobility Particle Sizer (SMPS). The data are consistent with a scaling relation of the form:

$$(\rho \times k)_{soot} = \tilde{\rho} \cdot (1-\varepsilon) \cdot f(\varepsilon) \cdot d_{pr}^2 \cdot SCF \qquad \text{Eq. 15}$$

where the porosity of the deposits follows a power law in terms of the Peclet number[12, 56]

$$\varepsilon(Pe) = 1 - (1-\varepsilon_\infty) \cdot (1 + \frac{Pe_0}{Pe})^{-n} \qquad \text{Eq. 16}$$

Eq. 16 generalizes earlier porosity-Peclet number power-law correlations[12] obtained at $Pe > 0.3$ down to the diffusion-limited deposition limit. Pe_0 is a characteristic cross-over Pe number defining the scale beyond which the convective mechanism will take over the diffusive mechanism of deposition, and ε_∞ the large Peclet number asymptote of the porosity. Using Eq. 16, the experimental data of **Fig. 12** can be collapsed on a single curve as shown in **Fig. 13**.

At sufficiently high values of the pressure drop,

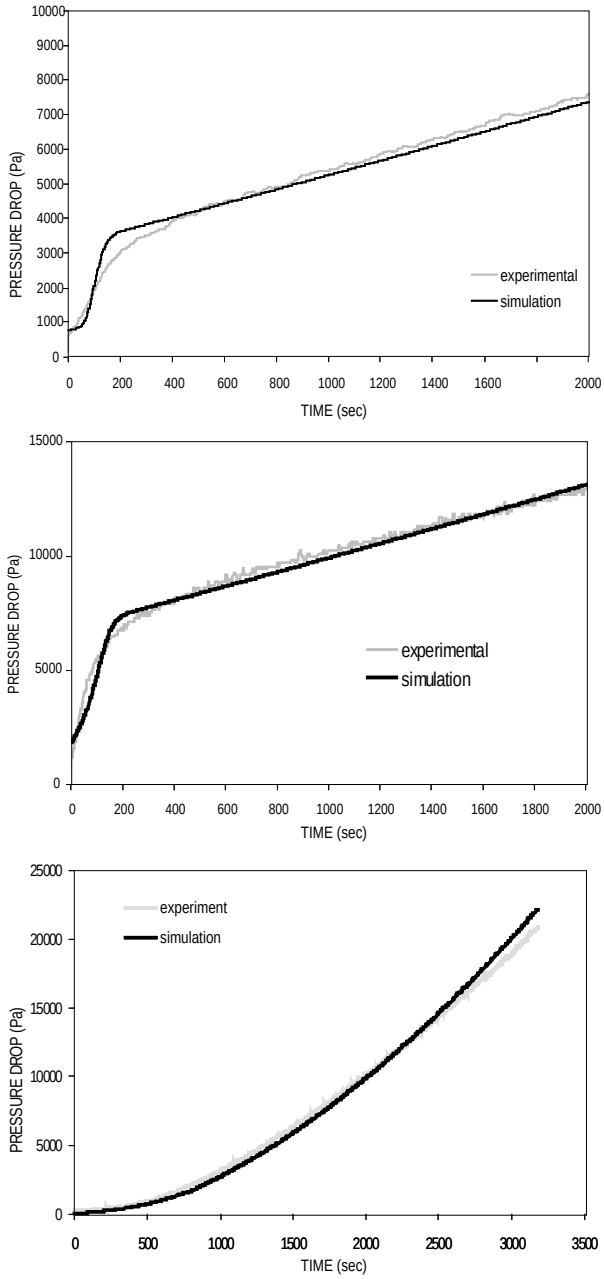

Fig. 10 Transient loading of a SiC (top), cordierite (middle) and fibrous metal (bottom) filter in the exhaust of a diesel engine. Experimental data and simulation results [42].

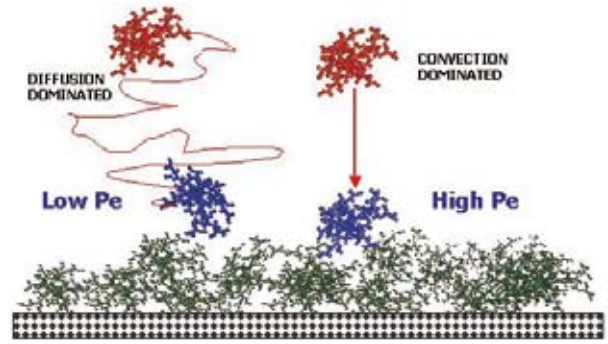

Fig. 11 Soot deposit growth mechanism: competition between diffusion- and convection-dominated growth, as determined by the Peclet number, leads to more porous deposits in the case of diffusion-limited deposition [12].

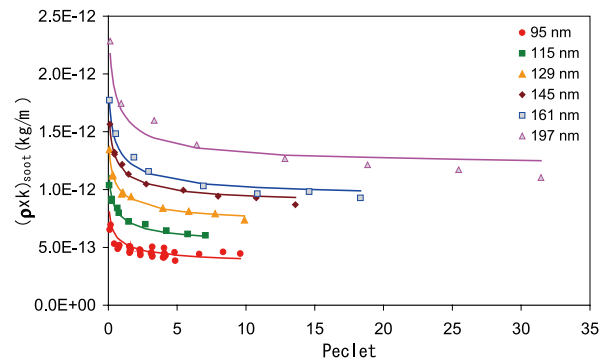

Fig. 12 Experimental measurements of CAST soot hydrodynamic resistance factor as a function of the Peclet number and aggregate mobility diameter. The continuous lines are plotted using the scaling relation form Eq. 15, Eq. 16 [47].

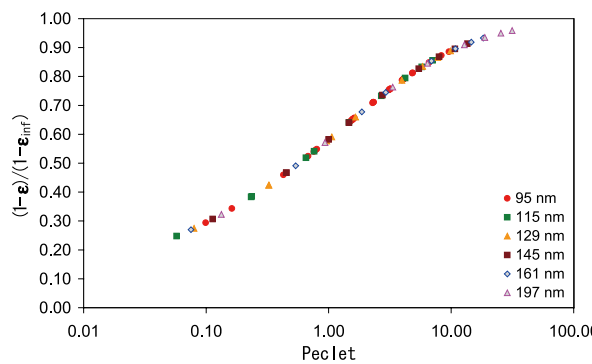

Fig. 13 Dependence of the soot cake porosity for different soot aggregate sizes at the prevailing Peclet number.

soot deposit compaction starts to set in. Konstandopoulos et al.[47] accounted for deposit compaction in the pressure drop model, treating the soot deposit as a Bingham-type of material that remains undeformed below a yield pressure and that deforms with a power law in the post-yield region:

$$\frac{\phi}{\phi_0} = \left(\frac{\Delta P - \Delta P_{cr}}{\Delta P^*}\right)^{\delta} \qquad \text{Eq. 17}$$

with ϕ denoting the solid fraction (1- ε) and ϕ the solid fraction of the deposit in the uncompacted stage. ΔPcr is the critical or yield pressure drop for the onset of deposit compaction, and ΔP^* is a scaling constant to make the equation dimensionally correct. The extended pressure drop model that accounts for deposit compaction was applied in[47] to obtain for the first time the evolution of the soot deposit microstructure under compaction. As shown in **Fig. 14**, critical pressure drops for the onset of compaction of soot

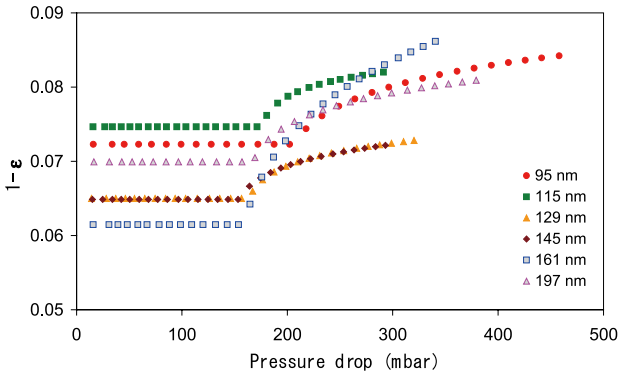

Fig. 14 Pressure-drop-induced compaction of soot cake deposits as a function of soot aggregate size.

cakes created by CAST-generated soot aggregates of different size are in the vicinity of 200 mbar and cause a gradual increase of the solid fraction (1- ε) of the compacted soot deposit, which can reach 25-30% for some aggregate sizes at high enough values of the pressure drop (> 400 mbar). These high pressure drops are non-typical for appropriately sized DPFs and under regular DPF operation, but it is possible to quantitatively take into account such phenomena if the need arises with the simple deposit compaction model mentioned above.

3.4 Effect of ash accumulation

The DPF pressure drop model has been extended to account for the presence of ashes in the channels of the DPF in[27, 47]. Ash deposit growth dynamics was described with a mechanistic model that exhibits different ash deposition profiles: deposition along the filter channel walls as well as deposition at the end of the filter channel. A comparison to experimental data available in the literature (**Fig. 15**) showed good quantitative agreement, and the model can be used to describe the dynamic ash transport and deposition phenomena inside the DPF.

Considering two idealized modes of ash accumulation, namely (i) ash only on the wall (forming a layer in series with the porous wall and the soot cake) and (ii) ash only at the end of the DPF channel (forming a plug that reduces the DPF length), it was possible to derive in[57] analytic approximations for the optimum cell density of wall-flow filters that minimizes the DPF pressure drop, under the combined constraints of a prescribed filter volume, exhaust flow, temperature, as well as different soot and ash loadings inside the filter, and thus to facilitate the task of selection and reliable employment of diesel particulate filters over the vehicle life-cycle.

4. The DPF as a Reactor

As already mentioned, modern DPFs need to be periodically cleaned (regenerated) in order to achieve efficient and safe operation of the vehicle. As typical diesel exhaust conditions are not hot enough to initiate and maintain particulate (soot) oxidation, active (engine) means are employed to raise the exhaust gas temperature up to the point that particulate oxidation can be self-sustained in the filter, and therefore the filter acts as a soot oxidation reactor. DPF regeneration can be achieved by employing a number of different approaches including direct and indirect catalytic measures ranging from fuel-borne catalysts (also known as fuel additives), generation of reactive species, catalytic combustion of post-injected fuel and filter coatings promoting soot oxidation, as discussed in the subsequent sections.

1) Regeneration measures

It is convenient to classify regeneration measures [31, 32, 33, 34] as active (employing external or engine means, see **Table 2**) or passive (usually employing catalytic means, although catalytic means can also be applied in active systems, see **Table 3**). Combinations of measures are also common.

2) Soot oxidation rate during regeneration

During regeneration tests with an increasing temperature, the pressure drop of the soot-loaded filters decreases and at the same time CO and CO_2 gases are emitted as the soot collected inside the filters oxidizes. In order to evaluate the regeneration behavior of different DPF technologies, the soot oxidation rate has to be calculated as a function of temperature. The normalized soot oxidation rate (s^{-1}) is defined as:

$$\dot{r}_{soot} = \frac{1}{m_0}\frac{dm}{dt} \qquad \text{Eq. 18}$$

where m_0 is the initial amount of soot mass collected. The soot consumption rate dm/dt is typically computed by adding the CO and CO_2 produced during the oxidation in a synthetic exhaust gas stream which does not contain CO or CO_2 in order to detect the soot-derived CO/CO_2. The evolution of the normalized soot oxidation rate as a function of temperature, an example of which is given in **Fig. 16**, provides a means to compare and evaluate different DPF technologies with respect to their soot oxidation activity. In addition, the CO selectivity which is defined as:

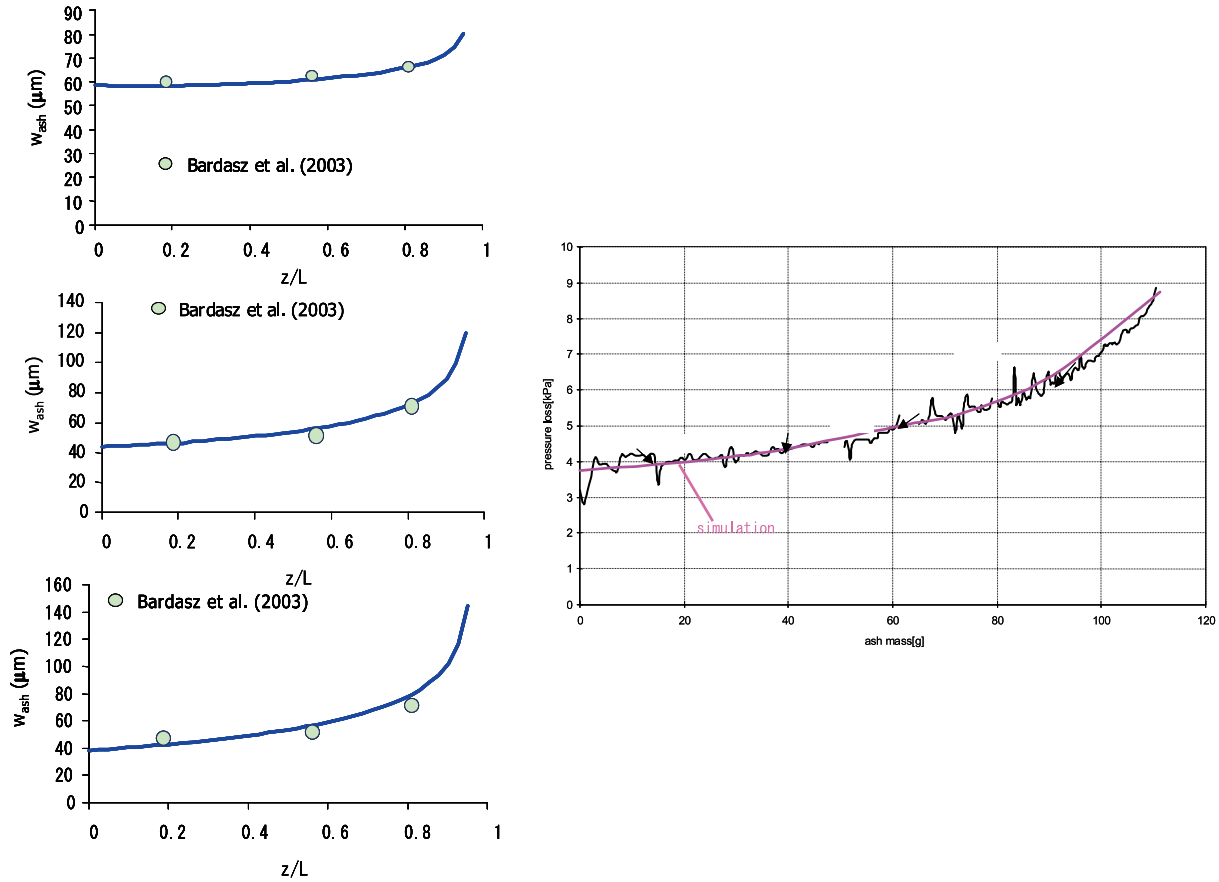

Fig. 15 Left: Simulated ash profile along the normalized filter length (z/L) vs. experimental data of Bardasz et al. with ash of different qualities, generated by high-sulfur oil doped into fuel (top), low-sulfur oil doped into fuel (middle), high-sulfur oil, regular use undoped into fuel (bottom). Right: Effect of ash accumulation on the DPF pressure drop. Experimental data courtesy of Ibiden Co. Ltd. and simulation results[47].

Table 2 Active Regeneration Measures

External means
• Fuel burners (full and partial flow)
• Electric heating (upstream or embedded in the filter)
• Microwave heating
• Injection of combustibles (e.g. fuel) in the exhaust
• Injection of catalytic and/or reactive species in the exhaust (e.g. H_2O_2[59])
• Generation of reactive species (e.g. non-thermal plasma [60])
• Electrochemical filter reactor [61]
Engine means
• Exhaust gas recirculation
• Post-injection of fuel
• Decrease of boost pressure
• Intercooler bypass
• Injection timing retard

Table 3 Passive Regeneration Measures

• Catalytic means
• Fuel-borne catalysts
• Catalytic filter coatings
• Reactive species generation (e.g. NO_2 [62])

$$f_{CO} = \frac{CO}{CO + CO_2} \qquad \text{Eq. 19}$$

can be also calculated. The CO selectivity is an important parameter because it affects the total heat release during regeneration.

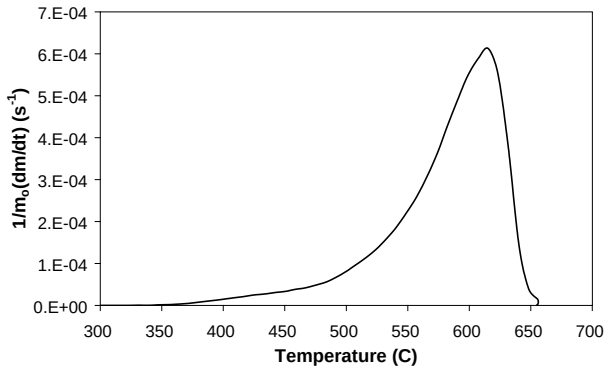

Fig. 16 Soot oxidation rate as a function of temperature.

3) Catalytic DPFs

The development of catalytic DPFs (CDPFs) aims at achieving:

(i) some soot oxidation activity under moderate exhaust temperature to prolong as much as possible the intervals between fixed regenerations, exploiting direct (i.e. through oxygen transfer) as well as indirect (through NO_2 generation) soot oxidation;

(ii) reduced soot ignition temperatures compared to uncatalyzed filters to allow for energy savings during regeneration;

(iii) tolerance to ash accumulation.

To achieve these goals, it is important to understand the different soot oxidation mechanisms and the significance of the soot-catalyst geometric proximity.

3.1 Catalytic oxidation mechanisms

Catalytic soot oxidation has a long history[63], while some recent reviews appear in[64, 65]. Catalyst chemistry is an important factor affecting the performance of a CDPF. Currently available CDPFs in the market feature predominantly catalytic coatings based on Pt-group metal (PGM) formulations aimed at oxidizing NO into NO_2 in order to achieve soot combustion at a lower temperature, motivated by the success of the CRT™ NO_2-assisted system[62]. The influence of NO_2 on soot oxidation, in conjunction with a highly selective NO to NO_2 oxidation promoting catalytic coating on a DPF, was studied experimentally and theoretically for the first time in[35]. At that time, NO_2-regenerative technologies were practiced with uncatalyzed filters[60, 62], and it was suggested that combinations of NO_2-regenerative technologies with catalytic filters could lower the dependence of NO_2-regenerative technologies on high engine-out NO_x concentrations, as NO_x emission standards become tighter. This has now become standard practice[60].

PGM-based CDPFs do not have a strong direct soot oxidation activity[11] and their operation depends on the balance between NO_2 and soot in the exhaust. It has nevertheless become clear from these developments that a noble metal such as Pt could have a beneficial role if used in conjunction with a direct soot oxidation catalyst, since Pt can also deliver "active oxygen" to the soot-catalyst interface in addition to oxidizing NO into NO_2.

Soot oxidation catalysts based on base metal oxides are thought to act through two mechanisms[64, 65].

(i) Redox mechanism: carbon oxidation is caused by lattice oxygen from the catalyst (reduction step) and re-oxidation of the catalyst by oxygen from the gas phase (oxidation step)

(ii) Spill-over mechanism: dissociation of adsorbed gas-phase oxygen over the catalyst surface occurs, followed by surface diffusion to the soot surface where carbon oxidation occurs.

The above mechanisms are not mutually exclusive and a soot oxidation catalyst can exhibit both.

Direct catalytic soot oxidation requires soot-catalyst proximity, a fact that has been known for almost half a century[66]. The problem of soot-catalyst contact in diesel emission control systems was recognized in the 1980s[63] as a barrier for active catalytic filter development, and it has become popularized in more recent laboratory studies of powdered carbon black-catalyst mixtures, with the introduction of so-called "loose" and "tight" contact[64, 65] samples. Direct demonstration of soot-catalyst contact effects on diesel soot oxidation in filters has been published in[67].

A mathematical description of the incomplete soot-catalyst contact, the so-called "Two-Layer Model" was introduced a decade ago, and it has been since incorporated into state-of-the-art DPF simulators[68, 69, 70, 71]. This forms the basic analysis tool that we employ in analysing soot oxidation rates in CDPFs as discussed in the next section.

3.2 The two-layer model of CDPF

Soot particle-catalyst contact is determined by the details of catalyst distribution in the filter (a type of "frozen" randomness) and the details of soot particle deposition and resulting deposit microstructure as well as soot deposit restructuring (a type of evolving randomness), it is therefore important to study it under realistic conditions, i.e. depositing fractal diesel soot aggregates from an engine under similar conditions of Peclet number, Pe[12]. The effect of Pe on the

soot deposit microstructure, soot-catalyst contact and reactivity is addressed in[72].

CDPF development has to address two key areas[67]: Chemistry and geometry and their interaction through the catalyst deposition process. The works in the literature dealing with chemistry at the powder synthesis level are too numerous to be cited here, while quantitative analyses of geometric effects have not been published as extensively. In the present work, in the geometric aspects of soot oxidation, we emphasize the kinetics in CDPFs by applying the two-layer formalism to analyze well-controlled direct catalytic soot oxidation experiments. **Fig. 17** depicts a schematic of the two-layer model[68]. Soot and catalyst coexist in a region (Layer I), on top of which a soot-only layer exists (Layer II).

Layer I: Catalyst-affected layer

As the catalyst coating can interpenetrate or overlap partially with the top part of the wall, we can define Layer I to be the region over which a spatial "field of catalyst activity" exists. Particles that oxidize when found within the "field of activity" are considered in contact with the catalyst. The fraction $\beta \in$ [0-1] of the soot surface in contact with the catalyst generally depends on the filter and coating structure and the deposition mode of soot in the filter. In general, β can vary dynamically due to reaction (oxidative fragmentation) and/or restructuring of soot microstructure. This layer can "store" a certain amount of soot (which depends on coating structure and filtration velocity) until it is filled up.

Layer II: Soot cake layer

This layer is formed by soot particles which form a "queue" on top of the filled-up catalyst-affected Layer I. These particles can locally migrate into the catalyst-affected layer depending on an interaction parameter $\xi \in$ [0-1]. This also depends on the filter and coating structure and can vary dynamically for the same reasons as β.

The interested reader can consult the original references for the mathematical formulation of the two-layer model[68]. A simple way, however, to understand the two-layer model dynamics is to consider the following system of kinetics in Eq. 20 and Eq. 21. In Eq. 20, m_1 is the mass of soot in Layer I, a fraction β of which reacts with a catalytic rate and the rest of it reacts non-catalytically (thermal oxidation). In Eq. (2), m_2 is the mass of soot in Layer II which is consumed by thermal oxidation, but which also migrates in proportion to the parameter ξ into any "open" space that becomes available in Layer I after some of the m_1 soot reacts.

$$\frac{dm_1}{dt} = (-k_{cat}\beta m_1 - k_{th}(1-\beta)m_1)(1-\xi) \quad \text{Eq. 20}$$

$$\frac{dm_2}{dt} = -(k_{th}m_2 + \xi(\beta k_{cat} + (1-\beta)k_{th}m_1)) \quad \text{Eq. 21}$$

In the simplest applications of the two-layer model, the parameters β and ξ are taken to be constant. The reaction constants are assumed to follow global modified Arrhenius forms[68], and for well-controlled experiments with negligible oxygen variation across the filter, they can be assumed to incorporate into their pre-exponentials the oxygen concentration as well as the surface area of the soot. The two-layer formulation can also describe a fuel-borne catalyst system considering only Layer I and setting m_2 and ξ equal to zero.

A number of filter structures have been catalyzed in-house with base-metal catalysts with a variety of coating technologies, aimed at direct catalytic soot oxidation. All filter structures had a disk form of 60 mm in diameter and they were loaded with soot under identical exhaust conditions in side-stream reactors, already described in the past[33, 73], and they were subsequently subjected to a slow temperature ramp (3℃/min) under a 10% O_2-in-N_2 atmosphere in order to study soot oxidation in them by following the evolution of CO and CO_2 and effecting overall carbon

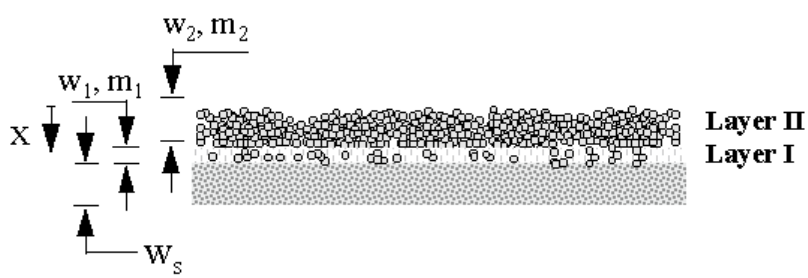

Fig. 17 Schematic illustrating the DPF wall, catalytic-coating-influenced Layer I and the top Layer II that is not in the sphere of influence of the catalyst.

balance.

For all the catalyzed materials there was a similar soot oxidation pattern. In **Fig. 18**, a typical soot oxidation rate curve for the aforementioned materials is depicted, where two regions of soot oxidation are observed. The first peak (in the region of 400-500℃), at lower temperature, originates mainly from the soot oxidized due to the soot-catalyst contact in Layer I, and the second peak, at a higher temperature, originates from the rest of the soot that is oxidized in Layer II. The first peak depends on the level of the contact that exists between the soot and the catalyst, whereas the second one occurs at the typical temperature range of thermal soot oxidation.

Fig. 19 demonstrates how the two modes of soot oxidation (catalytic and non-catalytic) add up to give the total soot oxidation behavior according to the two-layer model.

It is clear that the first peak results from the soot that already exists in contact with the catalyst in Layer I as well as from contributions of soot which migrates from Layer II into Layer I. The double peak is therefore a direct manifestation of the importance that catalyst layer geometry plays in establishing different modes of contact between the deposited soot particles and the catalytic coating. It is not possible to explain this double peak structure of the soot oxidation curves with a model based only on chemistry, since uncatalyzed soot oxidation exhibits a single peak and the same is true for mixtures of soot-catalyst powders[67].

An example of application of the two-layer model to analyze the soot conversion on a catalytic filter is shown in **Fig. 20**, while **Fig. 21** demonstrates the ability of the two-layer model to describe the soot oxidation of several catalytic filter samples to within +/-5%[74].

The reduced activation energy (E/R) for the thermal oxidation for these samples is in the range of 21000 – 22000 (K)[74], and it is within the values usually reported in the literature, e.g.[63, 64, 65, 66, 67]. Catalytic oxidation activation energies are almost the same or up to 15% lower, and depend on the type of catalyst and coating technology employed[74]. Depending on the catalyst coating technology, the state of soot-catalyst contact expressed by β can span a large range

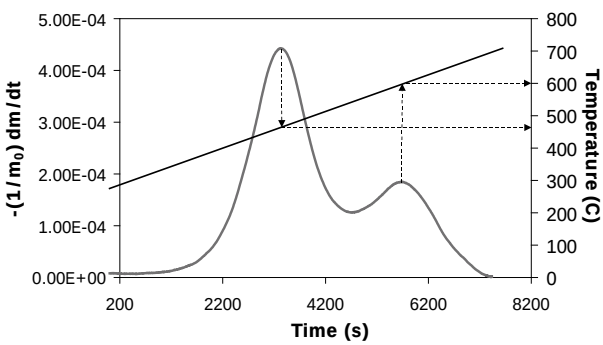

Fig. 18 Soot oxidation rate on catalyzed filter.

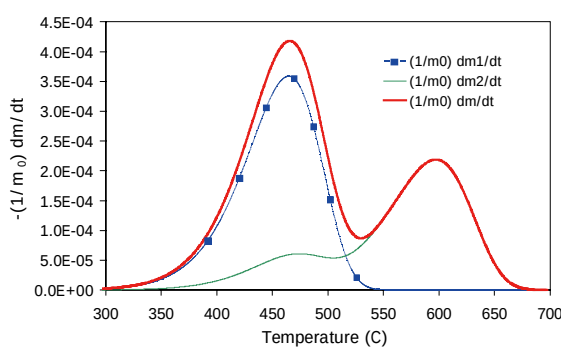

Fig. 19 Soot oxidation based on the two-layer model.

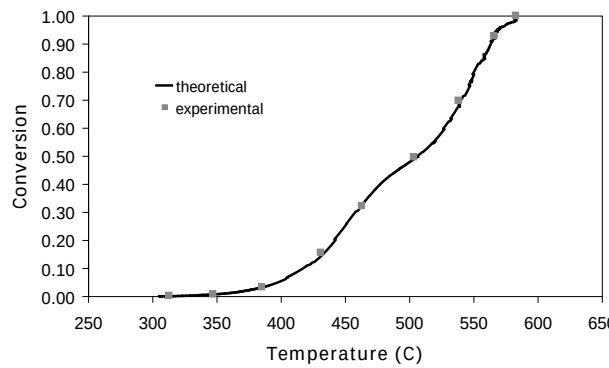

Fig. 20 Application of the two-layer model to experimental data for a catalyzed filter sample [74].

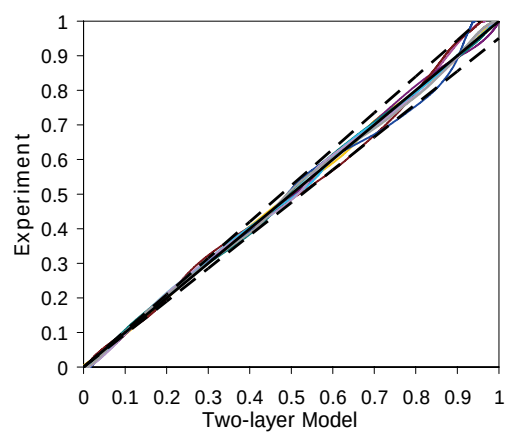

Fig. 21 Comparison of experimental data on soot conversion with the two-layer model. The dotted lines correspond to the +/- 5% spread from the line of perfect agreement.

(values of β from 0.0006 up to 0.214 have been measured in[74]), while migration of soot from Layer II into the catalyst-affected Layer I can occur with a varying degree of intensity as measured by the ξ parameter, which is measured to range from 0 (no migration) up to 0.642[74]. These findings demonstrate the important effect that the filter/catalyst micro-structural environment can have on the global oxidation kinetics. Essentially, it is possible to oxidize a small amount of soot in the catalyst-affected Layer I and still obtain a sufficiently high macroscopic reaction rate provided that the migration of soot from the top Layer II can proceed at an appropriate rate[74].

3.3 Catalyst formulations

Following the results of basic research on catalysts, e.g.[64, 65, 75, 76, 77, 78, 79, 80], we have embarked on a program of synthesis and screening soot oxidation catalysts with the goal of depositing them on filters. Numerous catalyst formulations with different characteristics have been studied[67] in order to arrive at a family of mixed oxide catalysts with high intrinsic soot oxidation activity, designated as E37. Although these catalyst formulations are proprietary and will not be listed here, the basic ingredient is cerium oxide doped with different rare earth and transition metals.

3.4 Catalyst deposition techniques

Catalyst deposition on the porous filter substrates can be performed either with a pre-formed catalyst powder slurry filtration procedure or by dipping the substrates into catalyst precursor solutions and subsequent firing. The coated filters are then thermally treated in a furnace. Permeability changes on the order of 15% can be noticed for filter samples coated by wet chemistry techniques[67].

We have introduced[81, 82] the aerosol spray pyrolysis technique (ASP), which combines catalyst synthesis and deposition on a porous substrate in one step, as an alternative to wet chemistry multi-step techniques (which include powder synthesis, slurry deposition and firing steps). The ASP procedure also has the advantages of precise control of the catalyst particle composition and of the quantity deposited, as well as its spatial deposition profile along the porous filter wall. An added benefit is the fact that the catalyst is deposited with the same mechanism as the soot particles, a feature which is expected to maximize the contact of the soot particles with the pre-deposited catalyst sites during filter operation.

In the aerosol spray pyrolysis technique, catalyst nanoparticles of controlled size are synthesized from the thermal decomposition/evaporation of precursor solution droplets introduced in a hot-tube aerosol reactor. Subsequently, these are deposited in-situ on porous substrates introduced in the reactor. Factors affecting the particle formation are the type of solution precursor, the temperature and the residence time in the reactor prior to deposition on the filter wall. Aerosol/vapor-phase techniques lead to nanostructured catalysts with controlled deposition profiles on the porous filter wall[67].

4) DPF Assessment in the exhaust

The assessment of CDPF technologies is ultimately performed by exposing full-size CDPFs on the engine exhaust and evaluating their regeneration behavior according to a certain methodology. In the present section, we provide an example of such an assessment, employing prototype in-house catalyzed full-scale DPFs, as well as a description of our testing methodology.

4.1 Engine and DPF characteristics

Full-scale DPFs were tested in the exhaust of a Euro III passenger car diesel engine (displacement 1.9 L, rated power 60 kW) with common-rail fuel injection, coupled to a servo-controlled dynamometer. The engine was operated under steady-state conditions as well as under transient conditions. Transient operation was achieved by simulating the speed and torque profiles of the New European Driving Cycle (NEDC) for the specific engine in the dynamometer, in collaboration with the engine manufacturer.

The characteristics of the DPFs (SiC wall-flow filters, 5.66 inches diameter × 6 inches long, 200 cells/in^2) in terms of their catalyst loading are shown in **Table 4**, and are denoted as DPF A-D. Overall, 4 catalyzed DPFs (at different loadings of the E37 catalyst in combination with a noble metal) were tested. An uncatalyzed DPF was also used as a reference. In **Table 4**, x is the amount of catalyst load (referred to as E37) and y is the amount of noble metal (NM) added in the filter. The noble metal is from the platinum group.

4.2 Regeneration method and control

Modifications of the engine tuning in conjunction with fuel post injection through the common rail system, EGR rate variation, boost pressure variation or throttling offers great opportunities to increase the exhaust temperature without adversely affecting fuel penalty and driveability conditions. Specific strategies

Table 4 Characteristics of the DPFs tested

DPF	Catalyst loading
A	No catalyst
B	E37: 2.7× / NM: 0y
C	E37: 1× / NM: 1y
D	E37: 2× / NM: 1y

that focus on a combination of boost pressure, EGR rate increase, and fuel injection modification have therefore been implemented by engine manufacturers [4, 11].

In some cases[83], the exhaust temperature is (in addition to engine measures) raised by exhaust-port fuel injection in front of a diesel oxidation catalyst (DOC). The same technique is also applied for some retrofit applications[84]. The applicability of the technique relies on having the DOC above the hydrocarbon light-off temperature (about 150 C), a condition,which is met with our test engine running over the NEDC, consisting of four city cycles and one extra urban (EU) cycle. **Fig. 22** shows the exhaust gas temperature of our engine over the cycle. As our Euro III test diesel engine has a "closed ECU" (i.e. a production ECU), we have selected exhaust port injection in front of a DOC as the means to raise the exhaust gas temperature, and in turn to effect regeneration of the DPF.

The exhaust port fuel injection set-up was constructed from standard automotive spare parts and consists of an air-assisted nozzle and auxiliary fuel and air pumps. Fuel flow to the nozzle is controlled by a custom electronic circuit defining the nozzle opening time and the period between injections. The fuel injection system has been optimized with the aid of a phase-Doppler analyzer in terms of droplet size. The fuel injection location was selected with the aid of CFD calculations so as to allow the fuel droplets to evaporate and the resulting diesel vapor to reach the DOC inlet with an even distribution. Fuel dosing and calibration of the system has been performed at representative engine operating conditions, and its effect on the increase of exhaust temperature has been studied providing an operational map.

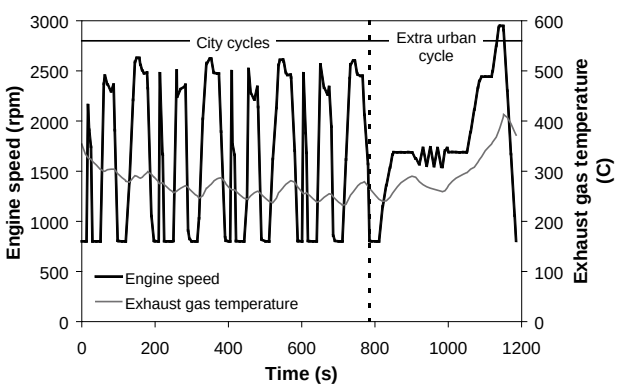

Fig. 22 Exhaust gas temperature and engine speed over the NEDC cycle.

Proprietary improvements in the virtual soot sensor include a detailed account of the effects of soot deposit microstructure under reactive and non-reactive conditions[12, 47] and emergency procedures in the case of virtual sensor failure (caused either by a hardware malfunction or by deviations from pre-programmed specific criteria and error bounds). When this occurs, regeneration would be initiated based on estimating the soot mass load from stored emission data.

4.3 Screening of DPF systems

The DPFs were tested in series with a DOC (Cordierite, 5.66 inches × 4 inches, 400 cells/in^2) in an exhaust set-up in order to study the influence of NO_2 in conjunction with the catalytic coating on soot oxidation.

Initial tests employed the DPFs A-D and an engine operating point where direct NO_2-soot oxidation was very low (due to a NO_x/soot ratio of 4) in order to test the ability of the catalytic coatings to deliver NO_2 to the soot collected inside the filter. The results of the DPF loadings at 2400 rpm and 6 bar brake mean effective pressure are shown in **Fig. 23**, while the soot mass load obtained from the virtual sensor is shown in **Fig. 24**.

As seen in **Fig. 24**, the presence of a DOC (hence NO_2 in the DPF inlet) causes an acceleration of soot oxidation with respect to the uncoated filter. Interestingly enough, DPF B - despite its zero noble metal content - exhibits continuous regeneration behavior very quickly, and this is maintained up to a challenge mass load of 8 g/m^2. This is attributed to the higher catalyst load (2.7×) it had with respect to the other filters. The thick porous coating creates an effective filter medium with soot and catalyst in close proximity, and at the same time provides the extra residence time for increased NO_2 turnover. DPFs C and D exhibit similar loading behavior with a progressively lower rate than the uncatalyzed DPF A.

The soot loading curves shown in **Fig. 23** indicate that the catalyzed DPFs B, C and D would reach a continuous regeneration state if they were exposed to the exhaust gas for sufficiently long periods, as a simple first-order reaction-deposition dynamic model would indicate[38]. These results demonstrate that the soot oxidation catalyst content as well as the noble

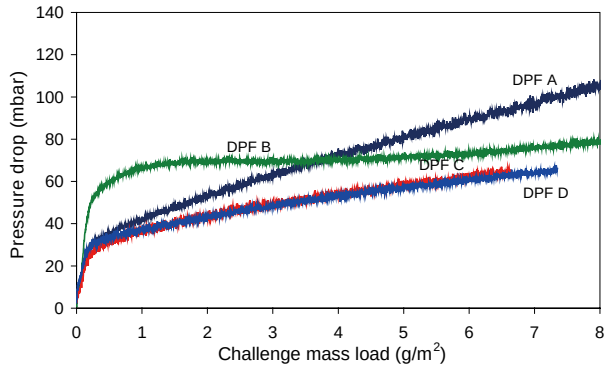

Fig. 23 Pressure drop of DPFs A, B, C and D as a function of challenge soot mass at steady state. DPF inlet temperature: 370 C, exhaust mass flow rate: 50 g/s, NO_x/soot ratio: 4.

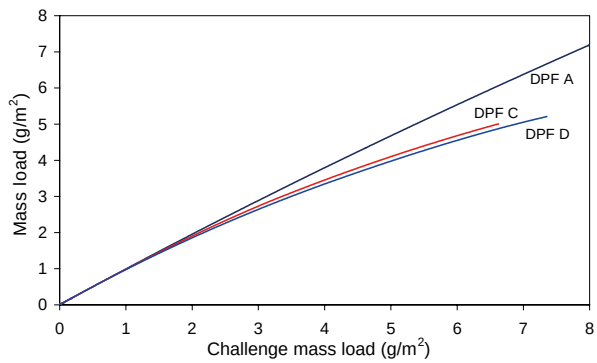

Fig. 24 Soot mass load of DPFs A, C and D at steady state. DPF B soot mass load is estimated to be close to zero. DPF inlet temperature: 370 C, exhaust mass flow rate: 50 g/s, NO_x/soot ratio: 4.

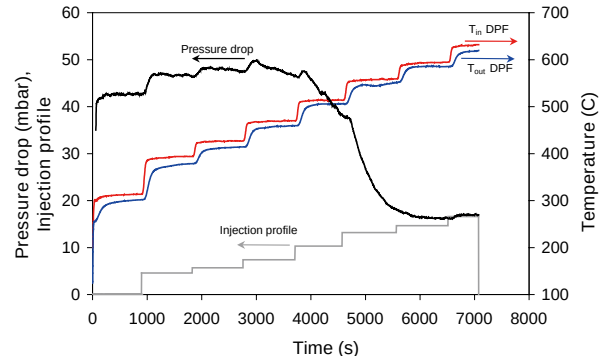

Fig. 25 Pressure drop and injection profile at stepped temperature soot oxidation for DPF B.

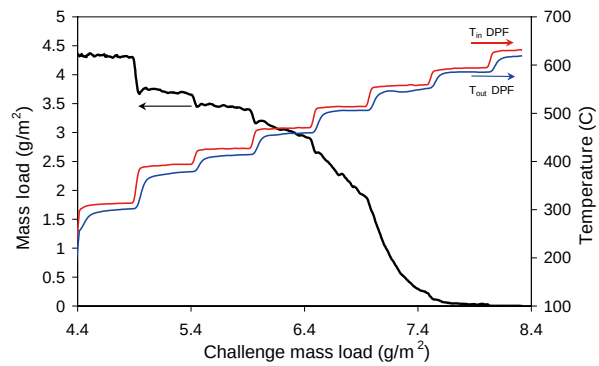

Fig. 26 Mass load calculated by the virtual soot sensor as a function of challenge mass load at stepped temperature soot oxidation for DPF B.

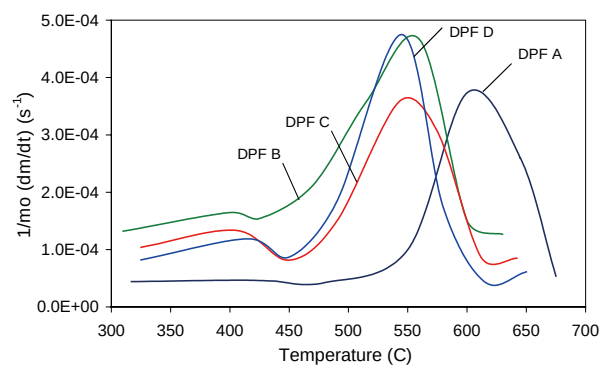

Fig. 27 Comparison of DPFs A-D over stepped temperature soot oxidation.

metal presence affect the DPF soot accumulation rate and need to be optimized, taking into account trade-offs between pressure drop, activity and cost.

The same DPF samples were also tested under a stepped temperature increase procedure to study their catalytic activity at higher temperatures. To this end, increasing quantities of engine fuel were injected upstream of the DOC in order to increase the exhaust gas temperature at the entrance of the DPFs, in steps of about 50 C. A representative result for DPF B is shown in **Fig. 25** in terms of DPF pressure drop and in **Fig. 26** in terms of soot mass load estimated by the virtual sensor.

The comparative assessment of the DPFs A-D in terms of the soot mass oxidation rate is shown in **Fig. 27**. It is evident that all DPFs exhibit significant and similar high temperature catalytic activity with respect to the uncatalyzed DPF A.

Based on these results, DPF C was chosen for subsequent study as an optimum compromise between catalyst load (directly affecting the cost and base system pressure drop), direct and indirect reactivity with NO_2 and a good catalytic reactivity at higher temperature with soot.

4.4 Transient Testing

The DOC-DPF C system was tested over a number of new European driving cycles in order to evaluate its behavior under transient conditions. With reference to **Fig. 28**, it is evident that the DPF exhibits

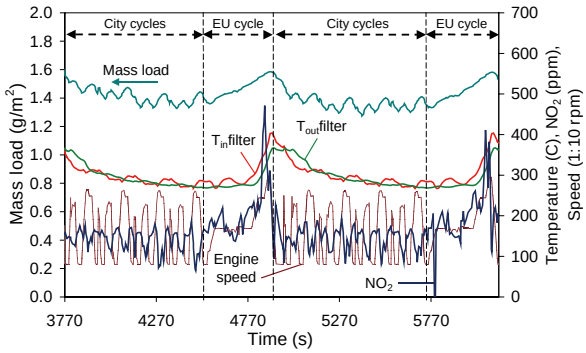

Fig. 28 Mass load variation under transient conditions during successive NEDCs.

good reactivity under NEDC conditions since the soot mass deposited in the DPF is oxidized when the exhaust temperature exceeds about 300℃ over the extra urban (EU) part of the cycle. The result is a very low rate of net soot mass loading of the system, which makes studies of soot accumulation extremely time-consuming.

To accelerate the loading process, DPF C was initially loaded without a DOC placed upstream up to soot mass loads of 8–10 g/m^2. Then the DOC was installed upstream of the DPF C and the system was subjected to exhaust-port injection schedules. By controlling the exhaust-port fuel injection rate and duration, it was possible to reach DPF temperatures in excess of 650-700 C and thus to apply varying amounts of external energy to the DPF at different points of the transient cycle. Examples of such tests are shown in **Fig. 29** and **Fig. 30**.

Fig. 29 depicts two successive fuel injections (each one with a duration of 2 min) performed at different soot mass load levels in the DPF, leading to partial regenerations. **Fig. 30** depicts a complete regeneration achieved by extending the duration of fuel injection to 33 min. Prolonged operation of the system would result in an increase of the "clean" DPF mass load due to the ash accumulation. The virtual sensor is programmed to take this into account by containing information on the flow resistance of ash-loaded filter materials[38].

Using such tests in conjunction with a state-of-the-art real-time DPF simulator [70, 71], it is possible to calibrate and to fully integrate model-based regeneration strategies with the soot virtual sensor module (see[86] for an early description of such strategies). Our current implementation relies on maintaining a target soot mass load in the DPF by injecting a quantity of fuel upstream of the DOC at appropriate instants. Since an exponential trade-off between the soot mass

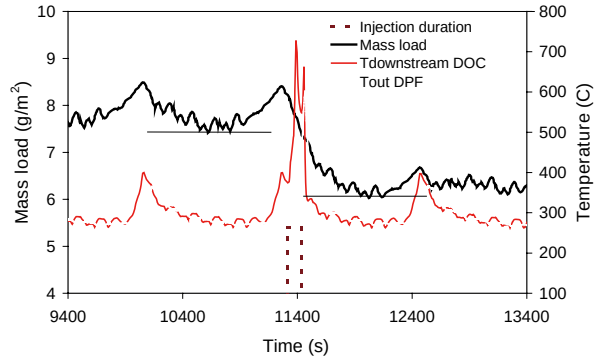

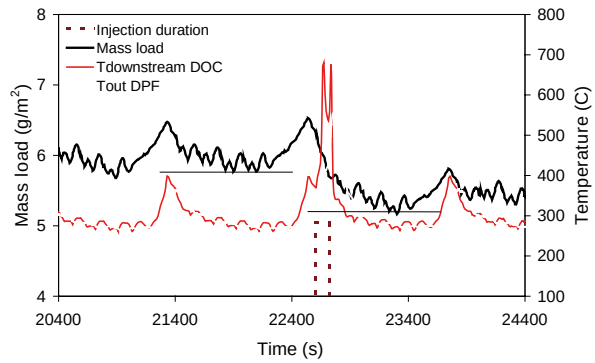

Fig. 29 Controlled regeneration over the NEDC by exhaust-port fuel injection initiated at different soot loadings of the DPF. Top: at 8 g/m^2. Bottom: at 6 g/m^2.

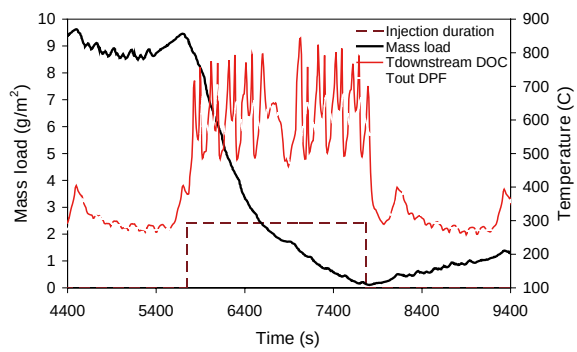

Fig. 30 Complete regeneration over the NEDC by exhaust-port fuel injection initiated at a soot loading of 9 g/m^2.

load in the DPF and fuel injection duration exists as shown in **Fig. 31**, it is evident that maintaining a target (constant) soot load in the DPF permits a priori optimization of the DPF size and cell density as well as significant fuel penalty savings.

As an example and based on our data with DPF C, we estimate that over the EUDC cycle, it is possible to maintain a target soot load of 5 g/m^2 with a fuel penalty of about 0.23% (a model-based controlled regeneration to bring the soot load whenever it reaches 6 g/m^2 down to 4 g/m^2). In comparison, a regeneration strategy that aims at a periodically completely

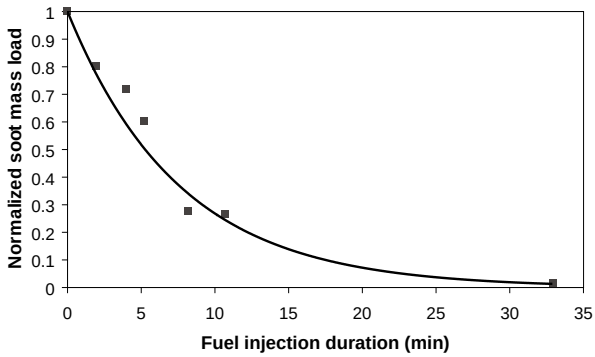

Fig. 31 Normalized soot mass load in the DPF vs. fuel injection duration.

cleaned DPF whenever the soot load reaches $10g/m^2$ would result in a fuel penalty of 0.52%.

Even though state-of-the art actively managed DPF systems[4] employing various aspects of the early virtual sensor models [50, 85] achieve impressively minimum amounts of fuel penalty (about 0.7%), it is clear that significant gains could be made by bringing novel and computationally fast simulation algorithms (also known as virtual sensors) into the developments of future ECUs.

5. Simulation Approaches to DPFs

Based on a traditional design of experiments approach, diesel particulate filter design, system integration and control becomes very time-consuming and costly due to the high number of tests required. This provides a privileged window of opportunity for the application of simulation. A recent review of advances in DPF simulation technology is given in [47, 87]. While the interested reader is encouraged to consult these references and their cited literature for more detailed information on the underlying assumptions regarding the treatment of the various physicochemical phenomena (including soot particle transport, deposition and oxidation), in the present paragraph we provide an overview of the mode of use of the different simulation models in practice.

The multiscale nature of the problem lends itself to a hierarchical organization of the different models. The models at each spatial scale are classified according to their complexity and detail in the representation of the actual situation. Three sub-models corresponding to the three size scales (wall, channel, entire filter) must be combined to give an overall simulation model of the DPF. Ideally, we would like to employ the most detailed treatment from each scale. Such an approach would thus entail a true-to-the-geometry description of the porous filter wall, along with a 3-D CFD simulation of each channel, coupled through conjugate heat transfer to the other numerous (on the order of a few thousand) channels of the DPF. As this is for obvious reasons impossible even with computing resources of the foreseeable future, the employed strategy is to use the most detailed models at each spatial scale in order to validate and extract parameters for simpler (lower-degrees-of-freedom) models applicable to the next scale. These relatively simple lower-order models are then connected with the hierarchically superior models in the next spatial scale, and the procedure is repeated over the entire DPF scale.

At the wall-scale algorithmic as well as process-based reconstruction techniques are employed to generate 3-D "digital materials" that are realistic representations of DPF microstructures. This is especially important for the development of new filter materials, the optimization of catalyst deposition inside the porous wall and for the design of gradient-functional filter microstructures where multiple functionalities in terms of particle separation and catalyst distribution (for combined gas and particle emission control) can be exploited. We refer to this approach as microflow simulation. Examples of computer-reconstructed DPF porous media are given in **Fig. 32** and encompass all currently available filtration media: extruded ceramic filters (including reaction-formed media as cordierite and grain-sintered media as SiC), fibrous filters, foams and sintered metal powder/wire mesh. Using the reconstructed porous material and Lattice Boltzmann-based methods (see e.g.[88]), the flow field inside the filter porous wall can be obtained. The computation of soot deposition in the filter wall can then be carried out based on iterations between convective-diffusion soot deposition and flow field updates (as the porous wall structure is being progressively blocked by the deposited soot)[47, 52]. An example of soot deposition in a granular-structured DPF "digital material" is shown in **Fig. 33**.

In practice, the detailed microflow simulation is employed when one is interested in developing new filter wall structures that need to meet specific requirements of flow resistance, filtration efficiency and catalyst coating accommodation. The models at this scale are therefore of the highest interest to the manufacturers of filter media. In this case, the majority of the experimental development revolves around small-scale filter samples, frequently in disk form, that are quite convenient for use in laboratory-scale experiments[35]. Depending on the outcome of this de-

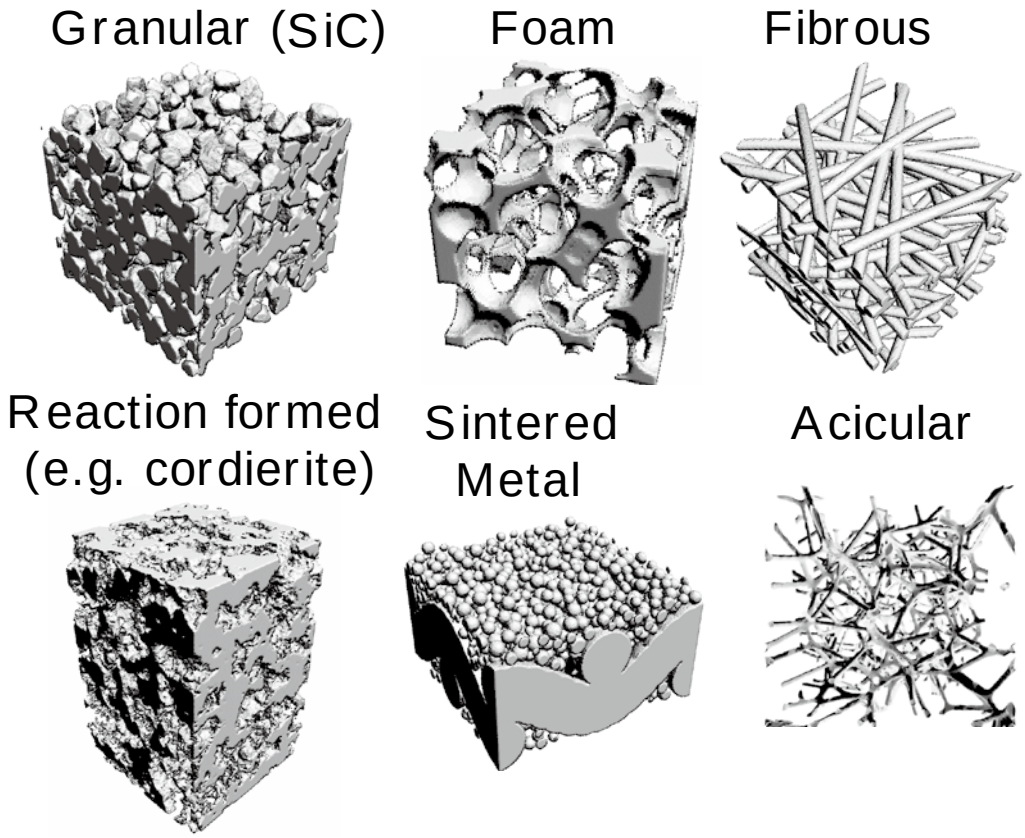

Fig. 32 Computer reconstruction of various porous filters.

velopment, interesting filter structures can be scaled-up into monolithic honeycomb samples. The use of a unit-cell structural description of the filter wall can be very advantageous at this stage, since with a minimal number of physically relevant parameters[35, 42] and well-characterized experiments, a description of the filtration and pressure drop behavior of the DPF can be achieved in a very computationally efficient manner. However, this information cannot be embedded directly into a filter channel simulation without significant computational resources, since the number of state variables needed for this is an order of magnitude higher. The already presented two-layer model in this case offers a compact description that can be embedded into a channel-scale simulation.

Channel-scale simulation is appropriate for the initial design and sizing of the DPF for an application. In this case, 3-D CFD is typically employed to assess the applicability of the classic perimeter-averaged approach[89], e.g. for filter channels of other shapes[44]. Otherwise, the single-channel perimeter-averaged formalism[30, 44, 89] represents a fast and accurate approach which can be employed in conjunction with well-defined experimental campaigns to obtain needed physicochemical parameters of the DPF in consideration. Single-channel simulation accounts for the majority of the simulation activities of the industry (DPF suppliers, catalyst coaters, emission control system integrators, engine manufacturers), and can provide useful estimates of axial soot loading distributions, pressure drop behavior and magnitude and location of temperature exotherms and thermal gradients during regeneration.

After the initial design phase, a DPF becomes part of an exhaust emission control system where its behavior also depends on the other components of the system. DPF models coupled with simulations of other emission control devices are then the appropriate tools to employ for system optimization and control. An example of a coupled simulation of a diesel oxidation catalyst (DOC) and a DPF in series is shown in **Fig. 34**. We observe how a hydrocarbon pulse injection upstream of the DOC raises the exhaust temperature and causes regeneration of the DPF. Such simulation tools are very useful for the development and optimization of post-injection strategies for DPF regeneration.

Important issues for the DPF performance at this

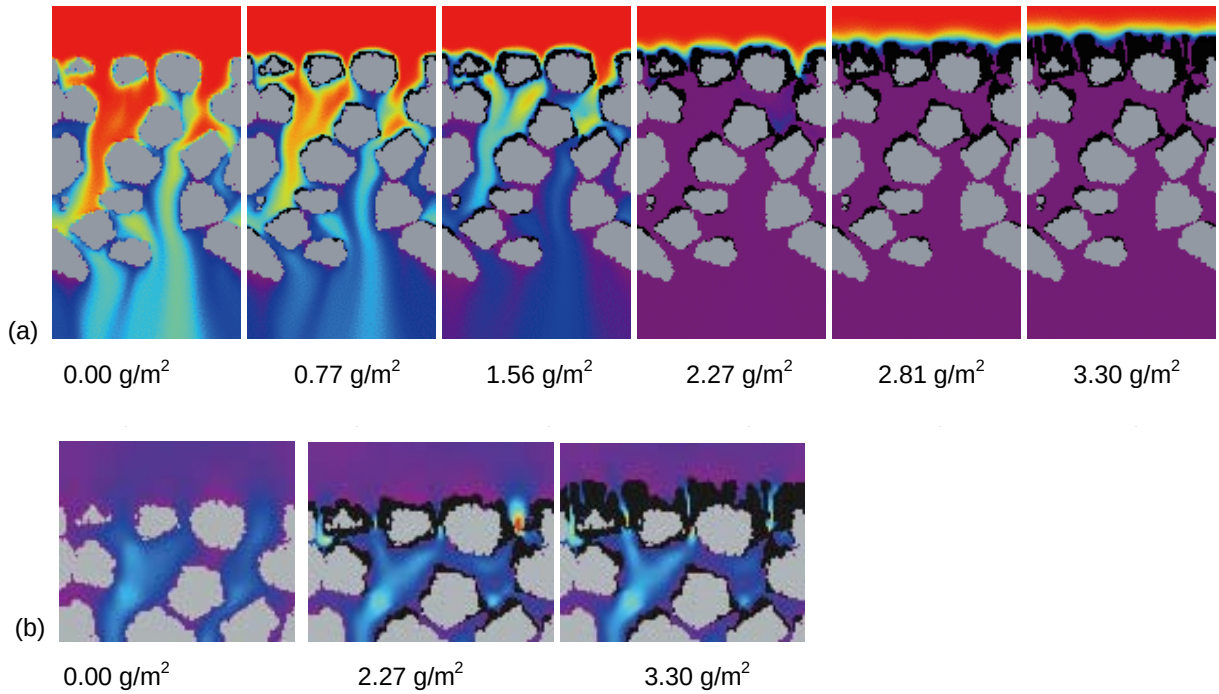

Fig. 33 Visualisation of soot deposition at different surface mass loads in an extruded ceramic (granular) filter wall. (a) Development of soot deposits (black) and soot mass fraction in the wall (solid material is gray) to the onset of cake formation. Soot mass fraction scale is from 0 (violet) to the inflow value (red). In (b), the velocity on a section through the filter wall is shown, with overlay of the soot deposit shapes.

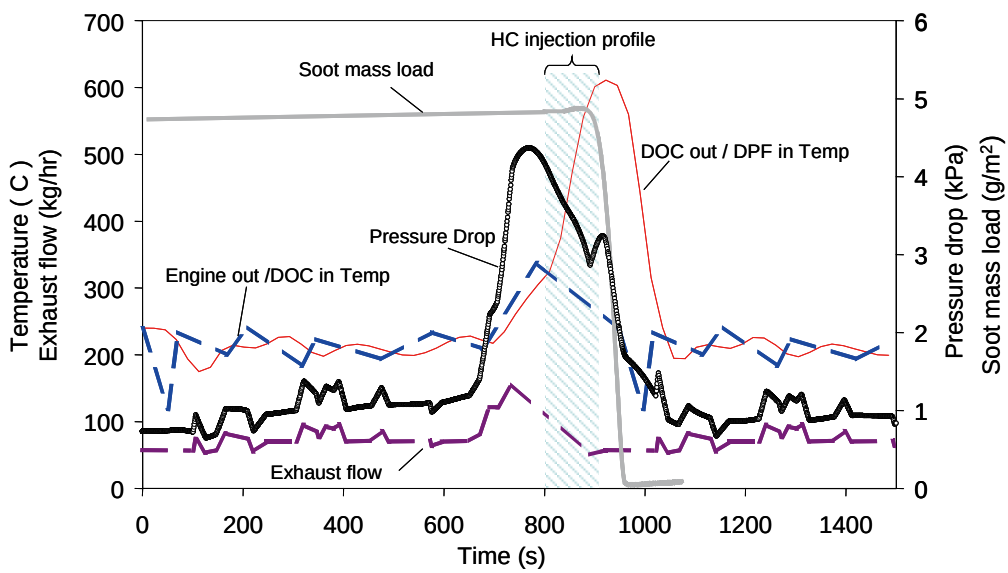

Fig. 34 Coupled DOC-DPF simulation. The 142mm × 152 mm, 200 cpsi SiC DPF regeneration is effected by hydrocarbon injection upstream of a 142mm × 152 mm 400 cpsi DOC over transient engine operation.

level are the development of transversal soot loading non-uniformities, induced by inlet cone flow and temperature maldistributions and/or by heat losses to the environment from the DPF external can surface. In addition, incomplete regenerations of the DPF need to be described. The continuum multichannel approach[69, 70, 71] represents a computationally tractable and accurate tool to address the previously mentioned issues. The development of highly integrated simulators of multi-functional exhaust emission control systems requires the interfacing of multichannel models of DPFs as well as other honeycomb-type con-

verters to standard 3-D computational fluid dynamics solvers. Recent advances in this area include the rigorous integration into the continuum multichannel framework of segmented filter designs, computationally efficient discretizations of non-axisymmetric filter geometries (e.g. oval and trapezoidal shapes), and intelligent coupling to general-purpose CFD solvers to account for spatial distributions of inlet conditions brought about by specific upstream exhaust piping layouts as well as to temporal variations caused by engine operation. An example of a 3-D simulation of a DPF is shown in **Fig. 35**.

While computing limitations still remain the barrier for the routine employment of detailed simulations of coupled emission control components over the entire exhaust system scale, we anticipate that in the near future such simulations will be widely employed by the industry, exploiting grid-computing environments. This means that from a research point of view, DPF simulation will focus on providing a deeper understanding and more detailed description of the coupled transport, structural and reaction phenomena occurring at the wall and pore scales, to permit materialization of the vision for an a-priori design of advanced microstructures, hosting multifunctional catalysts for the highly compact and efficient emission control devices of the future.

6. Conclusions

The diesel particulate filter (DPF) has evolved into the most complex emission control device, due to its multiscale and multitemporal operational nature in combination with the different functionalities (particle separation/gas and particle catalytic reactions) embedded in it. Despite the challenges offered by this state of affairs, it has been possible to develop a systematic understanding of the science and technology of DPFs. Our starting point has been fundamental studies of diesel soot particle size, composition and morphology, and the mechanisms that determine the microstructural properties of soot deposits in DPFs. Filtration efficiency, pressure drop, ash accumulation and soot reactivity (with emphasis on catalyst-assisted soot oxidation) were then addressed, employing experimental methodologies ranging from small-scale filter set-ups to full-scale devices installed in the exhaust of diesel engines. The experimental methods are complemented by computational approaches that range from true-to-geometry representations of porous DPF microstructures up to entire emission control system simulations. Properly combined, the current state of knowledge, experimental methods and simulation approaches provide a rational and systematic route for enhancing the design

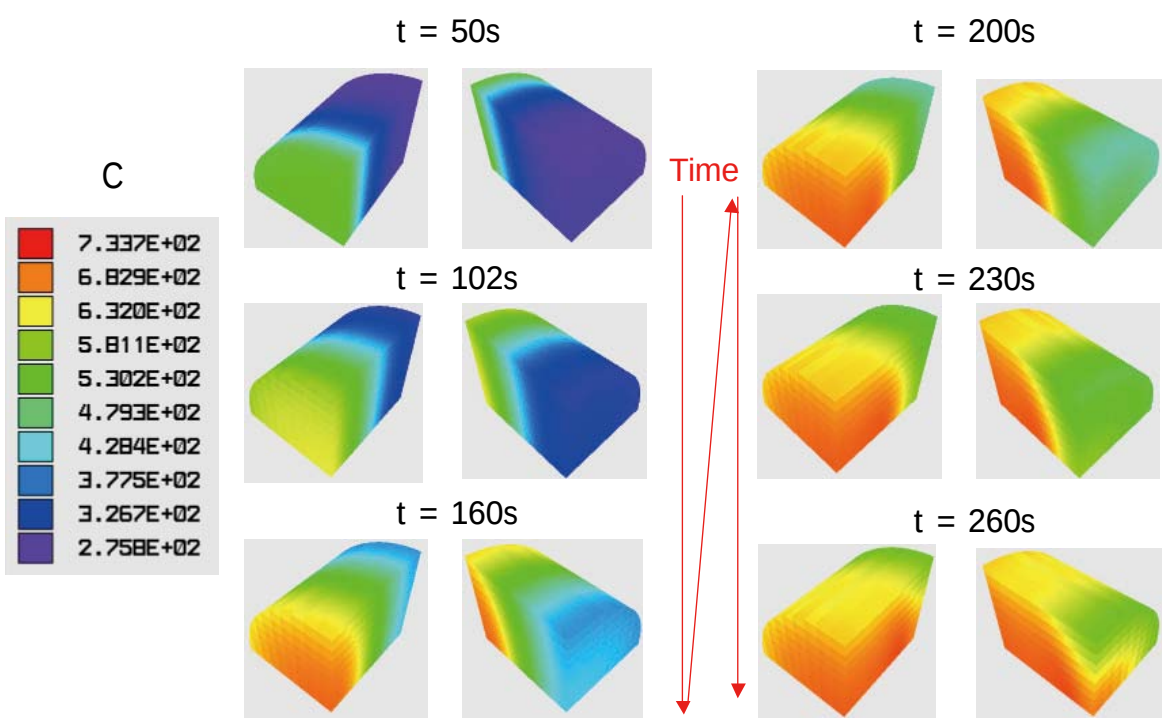

Fig. 35 3-D -DPF simulation. Example of of temperature field evolution in a 11.25 in × 12 in DPF during regeneration.

and reliability of future diesel particulate emission control systems.

Acknowledgements

Our work in the diesel emissions area has been supported in part by the European Commission framework programs through industrial collaborative projects DIDTREAT, CERFIL, MULTISENS, ART-DEXA, PSICO-DEXA, SYLOC-DEXA, STYFF-DEXA, FLOWGRID, IMITEC, COMET, MAAPHRI, IPSY, PAGODE, TOP-EXPERT, ATLANTIS, the Hellenic General Secretariat for Research and Technology through collaborative projects EPET-II, PAVE, EPAN and by a number of automotive industries and their suppliers. We are very grateful to them as well as to our colleagues at the APT Laboratory for all their hard work and support during these years. This paper is dedicated to the memory of our dear colleague Dr. Michael Claussen of CUTEC GmbH /University of Clausthal, Germany.

References

1) Ogyu, K., Ohno, K., Hong S. and Komori, T. (2004): Ash Storage Capacity Enhancement of Diesel Particulate Filter, SAE Tech. Paper No. 2004-01-0949.
2) Young, D.M., Hickman, D.L., Bhatia, G. and Gunasekaran, N. (2004): Ash Storage Concept for Diesel Particulate Filters, SAE Tech. Paper No. 2004-01-0948.
3) Bardon, S., Bouteiller, B., Bonnail, N., Girot, P., Gleize, V., Oxarango, L., Higelin, P., Michelin, J., Schuerholz, S. and Terres, F. (2004): Asymmetrical Channels to Increase DPF Lifetime, SAE Tech. Paper No. 2004-01-0950.
4) Boretto, G., Imarisio, R., Rellecati, P., Barucchi, E. and Sanguedolce, A. (2004): Serial Application of a Catalyzed Particulate Filter on Common Rail DI Diesel Engines For Passenger Cars, F2004V068, FISITA World Automotive Congress, Barcelona, Spain, May 23-27, 2004.
5) Nakatani, K., Hirota, S., Takeshima, S., Itoh, K., Tanaka, T. and Dohmae, K. (2002): Simultaneous PM and NOx Reduction System for Diesel Engines, SAE Tech. Paper No. 2002-01-0957.
6) http://www.greencarcongress.com/2006/01/mercedes_to_int.html
7) http://world.honda.com/news/2006/c060925DieselEngine/
8) Burtscher, H. (2005): Physical characterization of particulate emissions from diesel engines: a review, J. Aerosol Science, 36 (7), pp.896-932.
9) Kittelson, David B. (1998): Engines and nanoparticles: a review, J. Aerosol Science, 29 (5-6), pp.575-588.
10) Konstandopoulos, A.G., Gratz, L.D., Johnson, J.H., Bagley, S.T.and Leddy, D.G. (1988): Ceramic Particulate Traps for Diesel Emissions Control-Effects of a Manganese-Copper Fuel Additive, SAE Tech Paper No. 880009, SAE Trans. 97 sec. 6 (J. Engines) pp.37-53.
11) Konstandopoulos, A.G., Zarvalis, D., Papaioannou, E., Vlachos, N.D., Boretto, G., Pidria, M.F., Faraldi, P., Piacenza, O., Prenninger, P., Cartus, T., Schreier, H., Brandstatter, W., Wassermayr, C., Lepperhof, G., Scholz, V., Luers, B., Schnitzler, J., Claussen, M., Wollmann, A., Maly, M., Tsotridis, G., Vaglieco, B.M., Merola, S.S., Webster, D., Bergeal, D., Gorsmann, C., Obernosterer, H., Fino, D., Russo, N., Saracco, G., Specchia, V., Moral, N., D'Anna, A., D'Alessio, A., Zahoransky, R., Laile, E., Schmidt, S. and Ranalli, M. (2004): The Diesel Exhaust Aftertreatment (DEXA) Cluster: A Systematic Approach to Diesel Particulate Emission Control in Europe, SAE Tech. Paper No. 2004-01-0694 (SP-1861).
12) Konstandopoulos, A.G., Skaperdas, E. and Masoudi, M. (2002): Microstructural Properties of Soot Deposits in Diesel Particulate Traps, SAE Tech. Paper No. 2002-01-1015, SAE Trans. 111 (J. Fuels & Lubricants), pp. 434-442. Also in SAE SP, 1673, Diesel Exhausts Emission Control, pp. 181-190.
13) Van der Wal, Yezerets Aleksey, Currier, N.L., Kim, D., and Wang, C.M. (2007): Study of diesel soot collected from diesel particulate filters, Carbon, 45 (1), pp.70-77.
14) Van der Wal, R.L. and Tomasek, A. J. (2003): Soot oxidation: dependence upon initial nanostructure, Combustion and Flame, 134 (1-2), pp.1-9.
15) Van der Wal, R.L. and Tomasek, A.J. (2004): Soot nanostructure: dependence upon synthesis conditions, Combustion and Flame, 136 (1-2), pp.129-140.
16) Higgins, K.J., Jung, H., Kittelson, D.B., Roberts, J.T., and Zachariah, M.R. (2002): Size-Selected Nanoparticle Chemistry: Kinetics of Soot Oxidation, J. Phys. Chem. A, 106 (1), pp.96 -103.
17) Jung, H., Kittelson, D. and Zachariah, M.R. (2004): Kinetics and visualization of soot oxidation using transmission electron microscopy, Combustion and Flame, 136, pp.445–456.
18) Ishiguro, T., Takatori, Y. and Akihama, K. (1997): Microstructure of diesel soot particles probed by electron microscopy - First observation of inner core and outer shell, Combustion and Flame, 108 (1-2), pp.231-234.
19) Ishiguro, T., Suzuki, N, Fujitani, Y. and Morimoto, H. (1991): Microstructural changes of diesel soot during oxidation, Combustion and Flame, 85 (1-2), pp.1-6.
20) Harris, S.J. and Maricq, M.M. (2002): The Role of Fragmentation in Defining the Signature Size Distribution of Diesel Soot, J. Aerosol Science, 33, pp.935–942.
21) Kostoglou, M. and Konstandopoulos, A.G. (2006): On the Size Distribution of Diesel Soot Aggregates Undergoing Coagulation and Fragmentation, IAC.
22) Konstandopoulos, A.G. and Kostoglou, M. (2003): Modeling of diesel particulate size distributions with

oxidative fragmentation and coagulation, ETH-Conference on Combustion Generated Particles.
23) Merrill, C.J., Lighty, J.S., Eddings, E.G. and Sarofim, A.F. (2004): Investigation of the Oxidation and Fragmentation of Soot in a Two-Stage Flat Flame Burner System Utilizing a Scanning Mobility Particle Sizer, Western States Section of the Combustion Institute, Davis, CA, March 29-30.
24) Meakin, P.(1998): "Fractals, Scaling and Growth Far From Equilibrium", Cambridge University Press; 1st edition (January 15, 1998).
25) Viscek, Tamas (1992): "Fractal Growth Phenomena", World Scientific Publishing Co Pte Ltd.
26) Julien, R. and Botet, R. (1987): "Aggregation and Fractal Aggregates" , World Scientific.
27) Kostoglou, M. and Konstandopoulos, A.G. (2004): Oxidative Fragmentation and Coagulation of Diesel Soot Aggregates, ETH-Conference on Combustion Generated Particles.
28) Park, K., Cao, F., Kittelson, D.B. and McMurry, P.H. (2003): Relationship Between Particle Mass and Mobility for Diesel Exhaust Particles, Environmental Science and Technology, 37, pp.577-583.
29) Van Gulijk, C., Marijnissen, J.C.M., Makkee, M., Moulijn, J.A. and Schmidt-Ott, A. (2004): Measuring diesel soot with a scanning mobility particle sizer and an electrical low-pressure impactor: performance assessment with a model for fractal-like agglomerates, J. of Aerosol Science, 35 (5), pp.633-655.
30) Konstandopoulos, A.G., and Johnson, J.H. (1989): Wall-Flow Diesel Particulate Filters - Their Pressure Drop and Collection Efficiency, SAE Transactions 1998, Sec. 3 (J. Engines), SAE Technical Paper 890405, pp.625-647.
31) Diesel Exhaust Aftertreatment(1999): SAE Special Publication, SP-1414.
32) Diesel Exhaust Aftertreatment(1998): SAE Special Publication, SP-1313.
33) Diesel Exhaust Aftertreatment(1997): SAE Special Publication, SP-1227.
34) http://www.dieselnet.com
35) Konstandopoulos, A.G., Kostoglou, M., Skaperdas, E., Papaioannou, E., Zarvalis, D. and Kladopoulou, E. (2000): Fundamental Studies of Diesel Particulate Filters - Transient Loading, Regeneration and Aging, SAE Tech. Paper No. 2000-01-1016, SAE Trans. 109 (J. Fuels & Lubricants), pp. 683-705. Also in SAE SP, 1497, Diesel Exhaust Aftertreatment, pp. 189-211.
36) Adler Joerg(2005): Ceramic Diesel Particulate Filters" Int. J. of Applied Ceramic Techn. 2 (6), pp.429–439.
37) Howitt, J. and Montierth, M. (1981): Cellular ceramic diesel particulate filter, SAE Paper No. 81104.
38) Konstandopoulos, A.G., Vlachos, N. , Stavropoulos, I, Skopa S., Schumacher, U.,Woiki, D. and Frey, M. (2005): Study of a Sintered Metal Diesel Particulate Trap, SAE Technical Paper No. 2005-01-0968, SAE SP, 1940, Diesel Exhaust Emission Control Modeling, pp.217-228. Also in SAE Trans. 114 (J. Fuels & Lubricants), pp.465-475.
39) Oh, S., McDonald, J., Vaneman, G., Hegedus, L. (1981): Mathematical modeling of fibrous filters for diesel particulate - Theory and experiments, SAE Paper No 810113.
40) Konstandopoulos, A., Skaperdas, E., Warren, J. and Allansson, R. (1999): Optimized filter design and selection criteria for continuously regenerating diesel particulate traps, SAE Paper No 1999-01-0468.
41) Auto Emissions Magazine(1999): Corning Inc., No. 14.
42) Vlachos, N., Housiada, P., Zarvalis, D. and Konstandopoulos, A.G. (2002): Transient Filtration and Pressure-Drop Behavior of Diesel Particulate Filters, in Particle Loading & Filtration Kinetics in Fibrous Filters, U. Karlsruhe, June 27-30, (2002).
43) Masoudi, M., Konstandopoulos, A.G., Nikitidis, M. S., Skaperdas, E., Zarvalis, D., Kladopoulou, E. and Altiparmakis, C. (2001): Validation of a Model and Development of a Simulator for Predicting the Pressure Drop of Diesel Particulate Filters, SAE Tech. Paper No. 2001-01-911, SAE Trans. 110 (J. Fuels & Lubricants), pp.650-656. Also in SAE SP, 1582, Diesel Emission Control, pp.153-160.
44) Konstandopoulos, A.G., Vlachos, N., Housiada, P. and Kostoglou, M. (2003): Simulation of Triangular-Cell-Shaped, Fibrous Wall-Flow Filters, SAE Tech. Paper No. 2003-01-0844, SAE Trans. 112 (J. Fuels & Lubricants), pp.680-690. Also in SAE SP, 1755, Diesel Emission Measurement and Modelling, pp.227-238.
45) Masoudi, M., Heibel, A. and Then, P.M. (2000): Predicting Pressure Drop of Diesel Particulate Filters - Theory and Experiment, SAE Technical Paper 2000-01-0184.
46) Floerchinger, P., Anderson, M., Hou, Z., Taubert, T., Steinbrueck, E. and Angelo, T. (2003): Prediction and Validation of Pressure Drop for Catalyzed Diesel Particulate Filters, SAE Technical Paper 2003-01-0843 (SP-1755).
47) Konstandopoulos, A.G., Kostoglou, M., Vlachos, N. and Kladopoulou, E. (2005): Progress in Diesel Particulate Filter Simulation, SAE Technical Paper No. 2005-01-0946, SAE SP, 1940, Diesel Exhaust Emission Control Modeling, pp.11-40.
48) Konstandopoulos, A.G. (2003): Flow Resistance Descriptors for Diesel Particulate Filters: Definitions, Measurements and Testing, SAE Tech. Paper No. 2003-01-0846 (SP-1755).
49) Konstandopoulos, A.G., Skaperdas, E. and Masoudi, M. (2001): Inertial Contributions to the Pressure Drop of Diesel Particulate Filters, SAE Technical Paper 2001-01-0909.
50) Skaperdas, E. and Konstandopoulos, A.G. (2001): Prediction of Diesel Particulate Filter Loading Behavior for System Control Applications, CD AUTO 2001, 3rd International Conference on Control and Diagnostics in Automotive Applications, 4-6 July 2001, Sestri-Levante, Italy.
51) Friedlander, S.K. (1977): "Smoke, Dust and Haze.

Fundamentals of Aerosol Behavior", Wiley-Interscience.
52) Vlachos, N.D. and Konstandopoulos, A. G. (2003): Digital Materials Methods for DPF Development, SAE Tech. Paper No. 2006-01-0260.
53) Merkel, G., Beall, D. M., Hickman, D.L., and Vernacotola, M.J. (2001): Effects of Microstructure and Cell Geometry on Performance of Cordierite Diesel Particulate Filters, SAE Technical Paper 2001-01-0193.
54) Ido, T., Ogyu, K., Ohira, A., Hayashi, M. and Ohno, K. and Konstandopoulos, A.G. (2005): Study on the Filter Structure of SiC-DPF with Gas Permeability for Emission Control, SAE Technical Paper 2005-01-0578.
55) Chi, T.(1989): "Granular Filtration of Aerosols and Hydrosols", Butterworths series in chemical engineering (Butterworth, Stoneham, MA, 1989).
56) Rodriguez-Perez, D., Castillo, J.L., Antoranz, J.C., Konstandopoulos, A.G. and Vlachos, N. (2004): Mixed ODE-MC Model for the Soot Cake Formation in a Square Section Filter, European Aerosol Conference EAC 2004, Budapest, Hungary, 6-10 Sep.
57) Konstandopoulos, A. G. and Kladopoulou, E. (2004): The Optimum Cell Density for Wall-Flow Monolithic Filters: Effects of Filter Permeability, Soot Cake Structure and Ash Loading, SAE Tech. Paper No. 2004-01-1133 (SP-1861).
58) Bardasz, E., Mackney, D., Britton, N., Kleinschek, G., Olofsson, K., Murray, I and Walker, A.P. (2003): Investigations of the Interactions between Lubricant-Derived Species and Aftertreatment Systems on a State-of-the-Art Heavy Duty Diesel Engine, SAE Tech. Paper No. 2003-01-1963.
59) Roth, P., Eckhardt, T., Franz, B. and Patschull, J. (1998): H2O2-assisted regeneration of diesel particulate traps at typical exhaust gas temperatures, Combust. Flame 115, p.28.
60) Lueders, H., Stommel, P. and Geckler, S. (1999): Diesel exhaust treatment-new approaches to ultra low emission diesel vehicles, SAE Paper No. 1999-01-0108.
61) Christensen, H., Dinesen, J., Engell, H. and Hansen, K. (1999): Electrochemical reactor for exhaust gas purification, SAE Paper No 1999-01-0472.
62) Hawker, P., Myers, N., Huthwohl, G., Vogel, H., Bates, B., Magnusson, L. and Bronneberg, P. (1997): Experience with a new particulate trap technology in Europe, SAE Paper No. 970182.
63) Murphy, M.J., Hillenbrand, L.J., Trayser, D.A. and Wasser, J.H. (1981): Assessment of Diesel Particulate Control - Direct and Catalytic Oxidation, SAE Tech. Paper No. 810112.
64) Van Setten, B. (2001): "Development of a Liquid Catalyst for Diesel Soot Oxidation", Ph.D Thesis, Technical University of Delft, Netherlands.
65) Neeft, J.P. (1995): "Catalytic Oxidation of Soot; Potential for the Reduction of Diesel Particulate Emissions" , Ph.D. Thesis, Technical University of Delft, Netherlands.
66) Hennig, G.R. (1962): Catalytic Oxidation of Graphite, J. Inorg. Nucl. Chem., 24, pp.1129-1137.
67) Konstandopoulos, A.G., Papaioannou, E., Zarvalis, D., Skopa, S., Baltzopoulou, P., Kladopoulou, E., Kostoglou, M. and Lorentzou, S. (2005): Catalytic Filter Systems with Direct and Indirect Soot Oxidation Activity, SAE Tech. Paper No. 2005-01-0670 (SP-1942).
68) Konstandopoulos, A.G. and Kostoglou, M. (1999): Periodically Reversed Flow Regeneration of Diesel Particulate Traps, SAE Tech. Paper No. 1999-01-0469.
69) Kostoglou, M., Housiada, P. and Konstandopoulos, A.G. (2003): Multi-channel Simulation of Regeneration in Honeycomb Monolithic Diesel Particulate Filters, Chem. Eng. Sci., 58, pp.3273-3283.
70) Konstandopoulos, A. G., Kostoglou, M. and Housiada, P. (2001): Spatial Non-Uniformities in Diesel Particulate Trap Regeneration, SAE Tech. Paper No. 2000-01-0908.
71) Konstandopoulos, A.G., Kostoglou, M., Housiada, P., Vlachos, N. and Zarvalis, D. (2003): Multichannel Simulation of Soot Oxidation in Diesel Particulate Filters, SAE Tech. Paper No. 2003-01-0839.
72) Konstandopoulos, A.G., Lorentzou, S. and Kladopoulou, E.: Convective-Diffusive Deposition and Diesel Soot Reactivity in Catalyzed Particulate Filters, to be submitted.
73) Konstandopoulos, A.G., Zarvalis, D., Kladopoulou, E. and Dolios, I. (2006): A Multi-Reactor Assembly for Screening of Diesel Particulate Filters, SAE Tech. Paper No. 2006-01-0874.
74) Konstandopoulos, A.G., Kostoglou, M., Lorentzou, S., Pagkoura, C., Papaioannou, E., Ohno, K., Ogyu, K. and Oya, T.(2007): Soot Oxidation Kinetics in Diesel Particulate Filters, SAE Tech. Paper No. 2007 01-1129.
75) Neeft, J. P., Van Pruissen, O.P., Makkee, M. and. Moulijn, J. A. (1997): Catalysts For The Oxidation Of Soot From Diesel Exhaust Gases II. Contact Between Soot And Catalyst Under Practical Conditions, Applied Catalysis B: Environmental, 12 (1), pp.21-31.
76) Badini, C., Saracco, G. and Serra, V. (1997): Combustion of carbonaceous materials by Cu–K–V based catalysts I. Role of copper and potassium vanadates, Applied Catalysis B: Environmental, 11 (3-4), pp.307-328.
77) McKee, D.W., Spiro, C. L., Kosky, P. G. and Lamby, E.J. (1985): Eutectic Salt Catalysts for Graphite and Coal Char Gasification, Fuel, 64 (6), pp.805-809.
78) Fino, D. (2003): "Diesel-Soot Catalytic Combustion" , Ph.D. Thesis, Politechnico di Torino, Italy.
79) Ciambelli, P., Palma, V., Russo, P. and Vaccaro, S. (2002): Deep Filtration and Catalytic Oxidation: An Effective Way for Soot Removal, Catalysis Today, 73 (3-4), pp.363-370.
80) Ciambelli, P., Palma, V., Russo, P. and Vaccaro, S. (2003): Redox Properties of a TiO2 Supported Cu-V-K-Cl Catalyst in Low Temperature Soot Oxidation, Journal of Molecular Catalysis A: Chemical, 204-205, pp.673-681.
81) Karadimitra, K., Papaioannou, E., Macheridou, G. and Konstandopoulos, A. G. (2001): Ceria Nanoparticle

Coated Filters for Soot Emission Control, PARTEC 2001, International Congress for Particle Technology, Nuremberg, Germany, 27-29 March.
82) Karadimitra, K., Lorentzou, S., Agrafiotis, C. and Konstandopoulos, A.G. (2004): Modelling of Catalytic Particle Synthesis via Spray Pyrolysis & In-Situ Deposition on Porous Materials, PARTEC 2004, International Conference for Particle Technology, Nuremberg, Germany, March 16 -18.
83) Hiratsuka, Y., Ishihara, M., Tanaka, M., Suzuki, J. and Takagi, N. (2004): The Latest Technology of Controlling Micro-Pore in Cordierite Diesel Particulate Filter for DPNR System, SAE Tech. Paper No. 2004-01-2028.
84) Edgar, B. (2004): Emission Control Systems and Components for Retrofit, and First-fit Applications, 10th Annual Diesel Emissions Reduction (DEER) Conference, Coronado, California, August 29–September 2.
85) Konstandopoulos, A. G. and Kladopoulou, E. (2003): A Virtual Sensor for On-Board Diagnostics and Control of Diesel Particulate Filters, CDAuto03A2028, CD AUTO 03, 4th International Conference on Control and Diagnostics in Automotive Applications, Sestri-Levante, Italy, 18-20 June.
86) Kladopoulou, E., Yang, S. L., Johnson, J.H., Parker, G.G., Konstandopoulos, A.G. (2003): A Study Describing the Performance of Diesel Particulate Filters During Loading and Regeneration - A Lumped Parameter Model for Control Applications, SAE Tech. Paper No. 2003-01-0842 (SP-1755).
87) Konstandopoulos, A.G, Kostoglou, M. and Vlachos, N. (2006): The multiscale nature of diesel particulate filters, International Journal of Vehicle Design, 41, pp.256-284.
88) Chen, S. and Doolen, G. (1998): Lattice Boltzmann Method for Fluid Flows, Ann. Rev. Fluid Mech., 30, pp.329-????.
89) Bisset, E.J. (1984): Mathematical Model of the Thermal Regeneration of a Wall-Flow Monolith Diesel Particulate Filter, Chem. Eng. Sci., 39, pp.1233-1244.

Appendix

With reference to **Fig. 36**, the DPF pressure drop is written as the sum of various components, each of which can be determined in closed form as shown below:

$$\Delta P = p_7 - p_1 = \underbrace{(p_7 - p_6)}_{contraction} + \underbrace{(p_6 - p_5)}_{inlet\ channel} + \underbrace{(p_5 - p_4)}_{soot\ layer} + \underbrace{(p_4 - p_3)}_{filter\ wall} + \underbrace{(p_3 - p_2)}_{outlet\ channel} + \underbrace{(p_2 - p_1)}_{\exp ansion} \tag{A.1}$$

$$\Delta P = \Delta P_{contraction} + \Delta P_{inlet\ channel} + \Delta P_{soot\ layer} + \Delta P_{filter\ wall} + \Delta P_{outlet\ channel} + \Delta P_{\exp ansion} \tag{A.2}$$

$$\Delta P_{expansion} = p_2 - p_1 = \sqrt{p_1^2 + \frac{8}{3}\frac{\zeta \dot{m}^2 RT}{MW}\frac{(a+w_s)^4}{V_{DPF}^2 a^2}\left(\frac{L}{a}\right)^2} - p_1 \tag{A.3}$$

$$\Delta P_{filter\,wall} = p_4 - p_3 = \sqrt{p_3^2 + \frac{\mu}{k_w}\frac{\dot{m}RT}{MW}\frac{(a+w_s)^2}{V_{DPF}a}w_s + \beta\frac{\dot{m}^2 RT}{MW}\frac{(a+w_s)^4}{2V_{DPF}^2 a^2}w_s} - p_3 \tag{A.4}$$

$$\Delta P_{outlet\ channel} = p_3 - p_2 = \sqrt{p_2^2 + \frac{\mu \dot{m} RT}{MW}\frac{(a+w_s)^2}{V_{DPF}}\frac{4FL^2}{3a^4}} - p_2 \tag{A.5}$$

$$\Delta P_{soot\ layer} = p_5 - p_4 = \sqrt{p_4^2 + \frac{\mu}{k_{soot}}\frac{\dot{m}RT}{MW}\frac{(a+w_s)^2}{2V_{DPF}}\ln\left(\frac{a}{a-2w}\right)} - p_4 \tag{A.6}$$

$$\Delta P_{inlet\ channel} = p_6 - p_5 = \sqrt{p_5^2 + \frac{\mu \dot{m} RT}{MW}\frac{(a+w_s)^2}{V_{DPF}}\frac{4FL^2}{3(a-2w)^4}} - p_5 \tag{A.7}$$

$$\Delta P_{contraction} = p_7 - p_6 = \sqrt{p_6^2 + \frac{4}{3}\frac{\zeta \dot{m}^2 RT}{MW}\frac{(a+w_s)^4}{V_{DPF}^2 a^2}\left(\frac{L}{a}\right)^2} - p_6 \tag{A.8}$$

$$\Delta P = \Delta P_{contraction} + \Delta P_{inlet\ channel} + \Delta P_{soot\ layer} + \Delta P_{filter\ wall} + \Delta P_{outlet\ channel} + \Delta P_{\exp ansion} \tag{A.9}$$

The total pressure drop computation accounting for compressibility effects is performed easily in a spreadsheet by a back-substitution scheme, employing Eqs. (A.1-A.9) in dreereverse order, i.e. starting the calculation from the downstream side, where the pressure p_1 is known, and continuing upstream for the calculation of the remaining components. In the above equations, $\dot{m}$ the exhaust mass flow rate, while MW is the exhaust molecular weight. The effect of compressibility is illustrated in **Fig. 36**, where the pressure drop for a DPF, calculated with the incompressible and the compressible approach, is shown.

A deviation is observed at values of pressure drop which exceed 15 kPa with the incompressible model resulting in an overestimation of the pressure drop by about 7%. A maximum pressure drop of 12-14 kPa is usually prescribed by vehicle manufacturers when sizing a DPF for a series application, therefore in most practically relevant situations, the analytic incompressible model can be applied with very good accuracy.

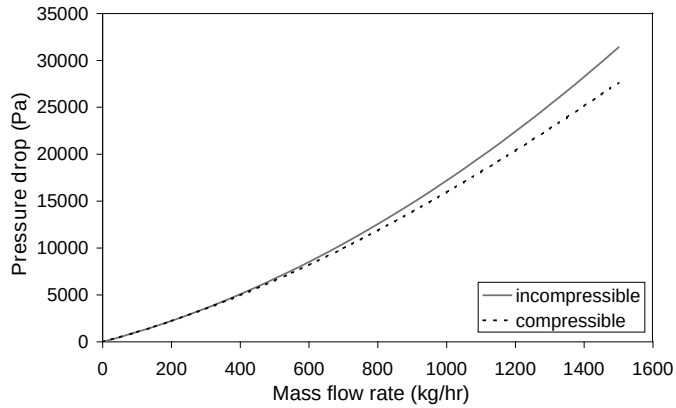

Fig. 36 Incompressible and compressible pressure drop model for a 5.66 in × 6 in, 181cpsi/14mil DPF, with $k=1\times10^{-13}$ m^2 and $\zeta=5$.

Author's short biography

Athanasios G. Konstandopoulos

Dr. Athanasios G. Konstandopoulos, Descartes Laureate (2006), is a specialist in combustion aerosols and nanoparticles. He is the Founder and Director of the Aerosol & Particle Technology (APT) Laboratory (http://apt.cperi.certh.gr) at CPERI/CERTH and a member of the faculty of Chemical Engineering at Aristotle University. He is the author of more than 100 scientific and technical papers and a Fellow of the Society of Automotive Engineers (SAE). He has a hybrid background in Mechanical (DiplME, Aristotle University, MSc Michigan Tech) and Chemical Engineering (MSc, MPhil, PhD, Yale University).

Eleni Papaioannou

Ms. Eleni Papaioannou is the Chief Operating Officer of the Aerosol & Particle Technology (APT) Laboratory (http://apt.cperi.certh.gr) at CPERI/CERTH. She has more than 12 years of professional engineering experience in nanoparticle emission control technologies and biological effects of nanoparticles. She has managed and technically supervised numerous collaborative projects of the APT Laboratory with the automotive industry and its suppliers. She is the author of 20 scientific and technical papers and she holds a Diploma in Chemical Engineering (Aristotle University).